EFDA–JET–PR(09)29

R.J. La Haye, D.P. Brennan, R.J. Buttery, S.P. Gerhardt
and JET EFDA contributors

Islands in the Stream: The Effect of Plasma Flow on Tearing Stability

Islands in the Stream: The Effect of Plasma Flow on Tearing Stability

R.J. La Haye[1], D.P. Brennan[2], R.J. Buttery[1], S.P. Gerhardt[3]
and JET EFDA contributors*

JET-EFDA, Culham Science Centre, OX14 3DB, Abingdon, UK

[1]General Atomics, P.O. Box 85608, San Diego, California 92186-5608, USA
[2]University of Tulsa, Tulsa, Oklahoma 74104 USA
[3]Princeton Plasma Physics Laboratory, Princeton, New Jersey 08540, USA
** See annex of F. Romanelli et al, "Overview of JET Results",*
(Proc. 22[nd] IAEA Fusion Energy Conference, Geneva, Switzerland (2008)).

Preprint of Paper to be submitted for publication in
Physics of Plasmas

ABSTRACT.

Reducing plasma flow clearly decreases the stability of tearing modes in multiple regimes (sawtooth, hybrid) in both high- and low-aspect-ratio tokamaks [DIII-D, J.L. Luxon, Nucl. Fusion **42**, 614 (2002); Joint European Torus, M. Keilhacker, Plasma Phys. Controlled Fusion **41**, B1 (1999); National Spherical Torus Experiment, M. Ono et al. Nucl. Fusion **40**, 557 (2000), each with distinct means of lessening rotation]. Further, reducing flow makes pre-existing "saturated" islands larger at the same beta (β). Thus lower plasma flow impairs high-beta operation owing both to the destabilization and to the impact of tearing-mode islands. Experimental results suggest that *flow shear* (not flow) at the tearing rational surface is classically stabilizing, making the effective tearing stability index Δ' of the total current density profile more negative (more stable). In this picture, with profiles and all else the same, the minimum metastable beta at which neoclassical tearing modes (NTMs) can destabilize is proportional to $-\Delta'$ and hence lower flow and flow shear lead to possible destabilization (depending on seeding) at lower beta. Similarly, if destabilized, the saturated NTM island width is proportional to $-\beta/\Delta'$ and thus increases as flow and flow shear are reduced. A working model gives a significant level of stabilizing shear if the plasma toroidal angular flow shear $-d\Omega_\phi/dr$ at a given rational surface is of order of the inverse of the product of the local values of the parallel magnetic shear length L_s and the Alfvén time τ_A. Experimental data are fitted for the effect of this normalization of flow shear in a simple empirical model for both onset and saturation of tearing modes. Most theoretical literature is on the consequence of flow shear on tearing stability at zero beta; tokamaks at high beta have large magnetic Prandtl number (an issue for the sign of the flow effect) and very large Lundquist number. It is in this regime that theory will be compared to experimentally based empirical models. The consequence for future tokamaks with low rotation may be lower tearing stability than now expected.

I. INTRODUCTION

The major instability limit to high beta operation of tokamaks [below the ideal magnetohydrodynamic (MHD) kink beta limit] comes from neoclassical tearing modes (NTMs) [1]. These modes are "classically stable" but destabilized by a helically perturbed pressure gradient driven current "bootstrap (BS) current". These islands "leak" energy radially [2]. Eddy currents induced by the rotating mode magnetic field perturbations in the vacuum vessel wall exert drag on the islands [3]: this can stop plasma rotation causing loss of the high confinement mode (H-mode). Most experimental studies of NTM onset and magnitude have previously been in tokamaks with substantial toroidal rotation Ω_ϕ in the direction of the plasma current I_p (co-I_p). Future large high field tokamaks, such as ITER, because of both large plasma inertia and low applied torque, will have relatively little plasma rotation. Of concern is how present experimentally based understanding of NTMs with high rotation will be different at low rotation. Low differential rotation could make NTM onset easier by reducing the shielding of seeding by other MHD events [4]. Low rotation could also act to lower (or raise?) the small island stabilizing polarization currents [5]. Once excited and "saturated", the size of an NTM island will in general be insensitive to the small island physics (transport, polarization, and/or ion banana width effects) due to the usually large hysteresis between initial growth at high beta and self-stabilization at low beta [6]. The resistive wall should continue to act as a perfectly conducting tearing stabilizing boundary for island rotations down to the inverse wall times which are quite low (50Hz in DIII-D). Plasma rotation can enter into the size of a large saturated island through the effective classical tearing stability of the total plasma current density profile; this is either through differential rotation (coupling of rational surfaces or of an island locked to another surface or island) or, as argued here, local flow shear. If large co-flow and thus plasma flow shear increases the

effective classical tearing stability, the beta for onset will be raised (subject to how the flow affects the seeding and the polarization threshold); the magnitude of a "large" saturated mode if excited will be reduced.

In this paper, we explore the experimental observations of how reducing plasma rotation causes NTMs to occur at lower beta and how these modes become larger. A new model is proposed. Where possible, it is pointed out where experiments suggest how rotation can actually be destabilizing. A prologue in Section II based on DIII-D [7] observations motivates the research; this includes how measurements are made with similar methods in NSTX [8] and JET [9]. The classical tearing and its importance for neoclassical tearing is discussed in Section III. The physics of flow shear on classical tearing is reviewed and a new empirical model presented in Section IV. NTM onset experiments in DIII-D, NSTX and JET are described in Section V, each with plasma rotation varied "shot-to-shot" by different means. In Section VI, the effect of flow shear on the "measured" Δ' through analyzing the changes in the saturated mode width in DIII-D is fitted for different situations and compared to the model of Section IV. A possible resolution of a sign effect of flow shear as an offset is discussed in Section VII. Conclusions and plans for both experiment and numerical modeling are presented in Section VIII.

II. PROLOGUE: COUNTER-NEUTRAL BEAM TORQUE CAPABILITY IN DIII-D

For the 2006 and subsequent DIII-D campaigns, a pair of counter (to I_p) neutral beams are available with the number of co (to I_p) beams reduced from seven to five. A plan view is shown in Fig. 1. Applying counter-torque to a previously all co-torque plasma with beta held constant by neutral beam injection (NBI) feedback is shown in Fig. 2 [10]. The plasma control system (PCS) maintains beta at a preset value by modulating the available injected neutral beam power, keeping the fraction of bootstrap nearly current constant. As the rotation

frequency of a pre-existing poloidal mode number $m=3$, toroidal mode number $n=2$ Mirnov mode (rotating island) was lowered, its amplitude increased. Further, the previously stable $m/n=2/1$ mode became unstable. Initial investigation focused on the increase in the $m/n=3/2$ mode amplitude. The NTM full island width w is proportional to the square root of the Mirnov amplitude. For saturated islands well above the size of the small island threshold, the island width is given by $w \approx -2\mu_0 j_{boot} L_q /(B_\theta \Delta')$ where j_{boot} is that fraction of the total local $q=m/n$ current density driven by the pressure gradient (or more precisely in terms including gradients in n_e, T_e and T_i), L_q is the radial magnetic shear length $q/(dq/dr)$, B_θ is the local poloidal field and Δ' is the classical tearing stability index (to be discussed) which is assumed stable, i.e., negative. The Mirnov amplitude could increase if: (1) the $q=m/n$ surface moved outboard closer to the outboard toroidal Mirnov probe array; but it does not, (2) if j_{boot} increased with counter-beams at fixed beta, but it actually goes down a little, or (3) if L_q increased or B_θ decreased, but they remain constant. The only choice remaining to explain the increase in $m/n=3/2$ amplitude $\tilde{B}_\theta$ is a reduction, less negative, in the value of Δ', a destabilizing effect of reduced plasma rotation. A less negative Δ' at $q=m/n=2/1$ would also explain the destabilization of an otherwise stable 2/1 NTM.

Before moving to Section III, some explanation of how measurements are made in DIII-D (similar to NSTX and JET) is in order. The MHD reconstruction code EFIT with the motional Stark effect (MSE) diagnostic of magnetic field pitch is used to locate rational surfaces, with an example shown in Fig. 3 [11]. This is in routine use. For more constrained and accurate reconstructions, kinetic data is added with ion and electron temperature, and electron density profiles (to be discussed). Rotation (usually only toroidal considered in the plasma core) is measured by charge exchange recombination (CER) with channels shown in Fig. 3 [12]. The profiles of Ω_ϕ versus major radius R for all co-beams (3425 ms) and near

balanced beams (3850 ms) are shown in Fig. 4 for a discharge to be discussed; $q = 3/2$ is noted and is the same at both times. The $m/n = 3/2$ mode at t = 3425 has a frequency 37.0 kHz and an amplitude of 4.0 Gauss; at t = 3850 it has slowed to 2.0 kHz and increased in amplitude to 9.7 Gauss. In this case, flow (rotation) shear has gone from a strong negative value to a weak positive value. Channel 5 gives a good match to the Mirnov frequency of the mode. Island width comes in general from Mirnov array analysis using EFIT [6,13]; this is calibrated by electron cyclotron emission (ECE) where possible with geometry given in Fig. 5.

The hybrid discharge whose rotation profiles are given in Fig. 4 (similar to 125492 of Fig. 2 but without an $m/n = 2/1$ mode) is 125476 and was chosen for detailed tearing analysis. The discharge is an upper biased double-null divertor configuration with upper triangularity δ_U = 0.64, lower triangularity δ_L = 0.40, safety factor at the 95% flux surface q_{95} = 4.1, minor radius a = 0.60 m, major radius R_0 = 1.75 m, plasma current I_p = 1.2 MA, axial toroidal field B_{T0} = 1.7 T, and normalized beta $\beta_N = \beta(\%)/(I/aB_{T0}) = 2.6$. Profiles from kinetic EFITs for times with all co-beams and with near balanced beams are shown in Fig. 6; the MSE diagnostic uses a self-consistent radial electric field E_r correction. There are no significant changes in the magnetic field reconstruction at $q = 3/2$ except for a little lower pressure which makes for a lower bootstrap current (13.0 A/cm^2 vs. 16.4) as computed with all terms by code ONETWO [14]. The difference in the profiles is too weak to explain the change in the island behavior (other than by rotation), regardless of the direction of change. It has previously been noted that Δ' is very hard to accurately calculate as gradients in J and q profiles are hard to resolve with sufficient accuracy [15].

These high quality MHD equilibrium reconstructions are run through the PEST-3 tearing stability code [16]. PEST-3 is used to determine the non-ideal linear stability of modes. The

outer solutions of the displacement field ($r < r_s$ and $r > r_s$) are matched at the $r = r_s$ resonance to form a matching Δ' matrix for the stability. In addition, PEST-3 returns a yes/no answer as to ideal stability. The equilibria must be ideal MHD stable to have a valid calculation of Δ'. The code does not have plasma rotation or the helically perturbed bootstrap current. As it is here run as a linear solver, the explicit nonlinear effects of finite islands are also not included. The code does not treat finite island physics, and flow only matters to the linearly perturbed solution when it is Alfvénic. However, PEST-3 will capture how the differences in equilibria, from the EFITs, affect the classical Δ'. The equilibria have q on axis $q(0) > 1$ at both times so that couplings of the $q = 3/2$ or 2/1 surfaces to $q = 1$ are not present. Even at the low rotation, it is assumed that differential rotation between the $q = 3/2$ and 2/1 (harmonic 4/2) surfaces is sufficient to decouple the surfaces, i.e., (3±1)/2 does not toroidally couple to 4/2 [4]. This choice for evaluation for Δ' in PEST-3 keeps the result obtained as simple as possible. With coupling included, the stability analysis becomes a matrix with off-diagonal elements for each mode toroidal coupling. Assuming differential rotation (between surfaces) satisfies a "perfect" wall condition [4]; the effective stabilizing wall can move in from the true conformal resistive wall (now taken as perfectly conducting in PEST-3) to the $q = 4/2$ surface for example (for the coupling of the $q = 2/1$ harmonic 4/2 to 3/2). Any wall stabilization for $q = 3/2$ would then be affected. This is a very easy condition to satisfy even at very low rotation. The results from PEST-3 for 125476 with mode $m/n = 3/2$ at the two times noted are that both times are linearly tearing (and ideal) stable. The values of dimensionless $\Delta' \psi_s^{2\mu}$ (PEST-3 usage for $\Delta' r$) are –0.68 and –0.21, respectively, at t = 3425 and 3850, with $\psi_s^{2\mu}$ a radial coordinate in flux space. As PEST-3 finds the linear classical Δ' is less stable at the lower rotation time with a little lower pressure and bootstrap current, an intermediate time (t = 3665) was also analyzed. This yielded $\Delta' \psi_s^{2\mu}$ = –0.66 in agreement with the all co-NBI high rotation time with the same beta and slightly higher bootstrap current density. The

PEST-3 calculations are summarized in Table I. For comparison, the linear Δ' is also available from these PEST-3 runs for $m/n=2/1$; note that at no time in 125476 is the 2/1 mode present. The 2/1 $\Delta'\psi_s^{2\mu}$ are respectively 0.04, –2.70 and –1.55 at the three times. Thus, PEST-3 finds the high rotation time closer to instability threshold. The PEST-3 $\Delta'\psi_s^{2\mu}$ values will be compared to "measured" $\Delta' r$ in Section VI.B.

We postulate that removing the flow shear (Fig. 4) decreases the effective classical tearing stability, an effect not in the ideal MHD outer region equations solved by PEST-3, making existing NTMs larger and onset of NTMs at lower beta, i.e., lower local bootstrap current density. This will be developed in the rest of the paper.

III. IMPORTANCE OF Δ' FOR NTMs

The classical tearing index Δ' represents the tearing stability of the total current density profile [17]. The standard value of Δ' (without an island or with flow shear effects) is calculated from the jump discontinuity at the rational surface in the logarithmic derivative of the perturbed magnetic potential; it has units of inverse meters in SI units. For $\Delta'<0$, the helically perturbed plasma has higher energy and the plasma is linearly stable as the perturbed energy $\delta W_{mag}\approx(-1/4\mu_0)(r\tilde{B}_r/m)^2\,\Delta' r>0$ where $\tilde{B}_r$ is the helical radial magnetic field perturbation at the $q=m/n$ surface of minor radius r. The normalized growth rate (the Rutherford equation) of an island of full width w is $(\tau_R/r^2)dw/dt=\Delta'$ where τ_R is the plasma resistive time [17,18]. For $\Delta'<0$, any classical island excited or driven by a transient would decay away. Δ' itself can be nonlinear, i.e., $\Delta'(w)$ through effects of finite w on the J and q profiles and by the need to match outer region solutions at $r=r_s\pm w/2$ rather than at $r=r_s$ (which itself assumes a very thin inner layer) [19,20]; for finite w, if $\Delta'(w=0)>0$ then the nonlinearly saturated ($\dot{w}=0$) island width $w\propto\Delta'(w=0)$. More on nonlinear saturation starting with linearly unstable modes as calculated from PEST-3 is developed in Ref. [21]. In

the rest of this paper, the effective classical Δ' is treated as including the effect on stability of rotation which can in particular raise or lower the perturbed energy in the Rutherford equation formulation.

The effective classical tearing index Δ' is a key parameter for high poloidal beta (β_θ), helically perturbed bootstrap current, destabilized NTMs. A simplified working relation is the modified Rutherford equation (MRE) developed from the pioneering idea of Ref. [22].

$$\frac{\tau_R}{r^2}\frac{dw}{dt} \approx \Delta' + \varepsilon^{1/2}\frac{L_q}{L_{pe}}\beta_{\theta e}\left(\frac{1}{w} - \frac{w_{marg}^2}{3w^3}\right) \quad , \qquad (1)$$

where $\varepsilon = r/R_0$ and $L_q = q/(dq/dr)$ are the local inverse aspect ratio and radial magnetic shear length respectively, $\beta_{\theta e} = 2\mu_0 k_B n_e T_e / B_\theta^2$ is the local electron beta poloidal and $L_{pe} = -p_e/(dp_e/dr)$ is the local gradient radial scale length in the electron pressure. The quantity w_{marg} is here simplified and incorporates all the small island stabilizing effects (transport, polarization and finite ion banana width) and is typically of order twice the ion banana width; $w_{marg} \approx 2\varepsilon^{1/2}\rho_{\theta i}$ where $\rho_{\theta i} \equiv (2m_i T_i / eB_\theta^2)^{1/2}$ [1,6]. Reference [1] gives a more general complete form of Eq. (1). Now j_{boot} is approximately dominated by electrons and is about $\varepsilon^{1/2} B_\theta \beta_{\theta e}/2\mu_0 L_{pe}$. If $\Delta' < 0$, the second term on the right-hand side in Eq. (1) is destabilizing and the origin of NTMs, and the third term makes for stability ($\dot{w} < 0$) at small $w < w_{marg}/\sqrt{3}$ [1]. Contours with typical parameters are shown in Fig. 7; the curves are $\dot{w} = 0$ for different $\Delta' r$ with growth ($\dot{w} > 0$) above the curves. Note that at the minimum at $w \approx w_{marg}$, the minimum beta needed for excitation of the metastable state without an island decreases as Δ' is made less negative [arrows in Fig. 7(a)]. Note also that at fixed beta, a saturated island $\dot{w} = 0$ gets larger as Δ' is made less negative [arrows in Fig. 7(b)]. In general, beta must exceed the minimum beta, a seed island w_{seed} must be applied to access the $\dot{w} > 0$ space, and the island saturates at a value $w > w_{seed}$. The scaling of the onset, i.e. critical, beta

thus involves a mix of the metastable space shown in Fig. 7, and the seeding and the effects are not separable, in general, from experimental data. The scaling of the minimum beta for excitation being possible tends to dominate the complete picture, leading, for example, naturally to a critical beta proportional to ρ_i^*, the ratio of localized Larmor radius at $q = m/n$ to plasma minor radius, which comes out of the polarization threshold being dominant [1].

The consequence of the classical tearing stability index Δ' on either the onset or the saturation of NTMs has potential to explain how plasma rotation (and particularly its shear) affects NTMs. Assuming everything else is the same (profiles, etc.): (1) existing islands ($\dot{w} \approx 0$) have $w \propto (\tilde{B}_\theta)^{1/2} \propto -1/\Delta' r$ and (2) the onset of islands ($\dot{w} > 0$) has beta at onset $\beta \propto -\Delta' r$. We look for Δ' as a function of local plasma flow and magnetic shears.

IV. PHYSICS OF FLOW SHEAR ON CLASSICAL TEARING

There is a rich theoretical literature on the effect of plasma flow and flow shear on classical tearing stability at zero beta, thus without the bootstrap current. Calculations vary widely as to: (1) regime and whether linear stability (i.e., growth) or nonlinear amplitude (i.e., saturation) are considered, (2) geometry is a slab or a circular cylinder, (3) only toroidal flow or only poloidal flow is assumed, (4) differential flow between different rational surfaces (a coupling issue) and/or local resonant surface flow shear are included, (5) flow effective in the outer "ideal" regions ($r < r_s$ and $r > r_s$) only, and/or only in the resistive layer, i.e., the inner layer in the absence of an island or within the island if present, and (6) either analytic theory or numerical modeling is done.

In tokamaks, islands tend to propagate near but not exactly at the local toroidal plasma flow; in this frame viscosity forces islands to propagate at about the magnitude of the ion diamagnetic drift frequency, a point to be addressed in detail in Section VII [23]. Poloidal

flow is typically negligible in the plasma core due to strong magnetic field asymmetry and thus drag in the poloidal direction. While flow can be transformed to zero by a choice of a frame moving with the island, radial flow shear remains, i.e., cannot be "transformed away." The applicability of any zero beta Δ' theory must be taken with care for tokamaks as to relevant regime; signs of flow and flow shear must also be checked with caution. The usual situation in tokamaks is co- to I_p-flow with a negative gradient as shown in Fig. 4 for "strong negative flow shear," and positive shear in safety factor q as inferred in Fig. 6 for $R > R_0$. The relevant regime for tokamaks is also very high magnetic Reynolds (Lundquist) number $S \equiv \tau_R / \tau_A \gg 1$ where τ_A is the inertial Alfvén time, here taken as $\tau_A \equiv (R_0 / B_{T0})(\mu_0 n_e m_i)^{1/2}$ where B_{T0} is the axial toroidal field, and high magnetic Prandtl number $P \equiv \tau_R / \tau_V \gg 1$ where τ_V is the viscous time, usually of order of the energy confinement time τ_E [24]. Note that $S \gg 1$ has the significance of "low" inertia in the island region so that the plasma conforms to the island helical magnetic field structure. Further away from the very narrow tearing layer, resistive tearing modes have the same characteristic time for field line bending as ideal MHD, i.e., τ_A. For $P \gg 1$, the flow conforms to the island structure. Thus, helical currents from deformed flow are sustained. As some theory is for $P < 1$, the perturbed flow would decay away, i.e., tend to vanish. Sufficient viscosity, i.e., $P \gg 1$, is needed for flow shear to be able to have an effect on the magnetic structure of tearing modes.

The toroidal rotation Ω_ϕ is obtained from CER measurement of CVI impurity lines, not from the main D ions. At high flow, this does not matter. However, any apparent sign effect in going from co- to counter-flow may be due to: (1) an offset from zero flow and/or flow shear in main versus impurity ion flow, (2) a non-zero gradient in poloidal flow, and/or (3) a frame for island flow in which at zero plasma flow the islands propagate close to the ion diamagnetic drift frequency [23]. This will be discussed in Section VII.

In Ref. [25], "Resistive tearing instability with equilibrium shear flow," it is found in a slab analytic calculation that when the flow shear is larger than the magnetic shear, the flow freezes the magnetic field and stabilizes the tearing mode. Shear flow influences the linear growth rate both through the outer and inner layers. However, viscosity is neglected so $P \equiv 0$.

In Ref. [26], "Resistive tearing mode instability with shear flow and viscosity," the linear slab calculation of Ref. [25] is extended to include viscosity. It is found that sheared poloidal flows can either increase or decrease the linear instability growth rate, depending on the viscosity, the magnetic shear, and the flow shear.

In Ref. [27], "Nonlinear evolution of resistive tearing mode instability with shear flow and viscosity," follows up Ref. [26] in the slab with sheared poloidal flow. Shear flow decreases the saturated magnetic island width. The shape of the flow profile is found to matter and the situation of zero local flow ($\Omega_\phi = 0$) but with local gradient $d\Omega_\phi / dr$ a maximum has the most significant effect. Here studies were made with S up to 10^5 and with P up to 10^3.

In Ref. [28], "Effect of sheared flows on classical and neoclassical tearing modes," toroidal velocity shear in a toroidal geometry is found to have a destabilizing effect. Numerical solutions of a set of reduced generalized MHD equations that include viscous force effects are made. However, perpendicular viscosity is not considered. Differential rotation between rational surfaces is found to be stabilizing.

In Ref. [29], "Effect of sheared equilibrium plasma rotation on the classical tearing mode," above a given threshold in the rotation shear (cylindrical geometry, toroidal plasma rotation only) a tearing mode unstable in the absence of rotation can be stabilized; rather than the absolute value of toroidal rotation, it is the local derivative that affects stability. The importance of both $S \gg 1$ and in particular $P \gg 1$ for a stabilizing effect is noted. Numerical

solutions are made for an $m/n = 2/1$ tearing mode at zero beta which is classically unstable without flow, i.e., $\Delta' > 0$. The growth rate $\gamma \tau_A$ is computed for sheared toroidal rotation with fixed profiles in different regimes of S and P. For $S \gg 1$ and $P \gg 1$, sufficient flow shear makes $\gamma \tau_A$ negative. The sign of the effect is opposite, i.e., destabilizing for $P \ll 1$, presumably because plasmas with low viscosity are "relaxed," i.e., stabilizing helical currents driven by the flow shear are damped. This is consistent with Ref. [28] in which the outer region flow shear is destabilizing. For $S \sim 10^7$ and $P \sim 30$ parameters typical of DIII-D for example, the stabilizing effect of flow shear is insensitive to values of S and P. As $\Delta' > 0$ without flow in these calculations, and γ becomes negative with sufficient flow, it is implied that the effective Δ' becomes negative, i.e., the state with the helical perturbation has a higher magnetic energy. A computation with $\Delta' < 0$ without flow would be of interest to see how the added flow shear affects the negative growth rate to confirm this.

A diagram illustrating how local flow shear can influence tearing drawn from the theory is shown in Fig. 8. Magnetic shear (with no flow shear) varies the field line pitch with q increasing with major radius as shown in Fig. 8(a). The arrows show the direction parallel to the magnetic field in the frame $q = m/n$ for the usual situation in DIII-D of toroidal field anti-parallel to toroidal plasma current. Resistive tearing can only occur because of the magnetic resonance at $q = m/n$. The magnetic radial shear varies the field line pitch; thus the singularity at the rational surface is limited in radial extent. The resonant condition $(1 - nq/m)$ becomes $-(r - r_s)/L_q$ which makes tearing "harder", i.e., it takes more energy to bend field lines, and this makes the linear classical Δ' from outer solution matching more negative, i.e., more stable. The diagram with flow shear added, Fig. 8(b), is for co-flow transformed away with the usually decreasing flow with major radius; the large arrows show the direction of the flow in this frame with zero flow at the island O-point. The island is

distorted as shown [30] due to the viscous drag of a sheared flow and the flow shear provides an additional means to limit the radial extent of the resonance. A perturbation phase can be defined as $\phi = n(Z + V_z t)/R - mx/r$, referring to Fig. 8. We assume only co-toroidal flow V_z, x/r is a poloidal coordinate (where poloidal flow could be added), and a left handed coordinate system as used in DIII-D, i.e., I_p opposite to B_T, Z in B_T direction, co-flow in I_p direction. The radial variation in the phase across the island (or across the inner tearing layer in the absence of the island) should go as $\delta\phi \propto \nu_\perp [d(V_z/R)/dr](r - r_s)$ where $\nu_\perp$ is the perpendicular viscosity [30]. Thus in conjunction with the radial magnetic shear $\propto L_q^{-1}$, the tearing resonance is limited. The effect of the phase variation with flow shear will be absent for $\nu_\perp \equiv 0$, thus explaining why $P = \tau_R/\tau_v \gg 1$ for a stabilizing effect is necessary in Ref. [29]. One can speculate that flow shear has the largest stabilizing effect through the inner layer physics (provided $P \gg 1$) and weaker or even destabilizing effects through the ideal outer regions as the rotation is sub-Alfvénic. Theory and modeling must be carefully considered, as previously discussed, as to which rotation physics effects are included and to which regime a plasma is in.

For test particles going parallel to $\dot{B}$ in the frame of $q = m/n$, the usual flow shear (co-flow peaked rotation profile) is additive in phase with the magnetic shear; for test particles going anti-parallel to $\dot{B}$, the effect is opposite. The shears are additive in the first case, and opposing in the second case. For counter-flow with the magnitude decreasing toward the wall, the sign of the flow shear becomes positive, i.e., big arrows in Fig. 8(b) flip sign. This could flip the sign of how flow shear adds to magnetic shear. But a source of the physics that breaks the symmetry between test particles going parallel or anti-parallel to $\dot{B}$ is needed, i.e. to have a sign effect of flow shear. An ion diamagnetic drift frame shift added to toroidal

flow could make for an offset for how the flow shear adds, rather than a true sign effect as co-flow is switched to counter-flow. This is discussed further in Section VII.

Without flow, the linear classical Δ' for zero island width is calculated by matching the outer solutions inside r_s and outside r_s at the rational surface. The "inner layer" at r_s is assumed thin and matching at the vanishingly thin inner layer determines the jump in $\psi'/\psi|_{r_s}$ (which is Δ') where ψ' is the radial gradient of the helically perturbed flux; this is the logarithmic derivative of ψ. The actual growth rate for $\Delta' > 0$ requires balancing resistive, inertial and viscous effects within the inner layer. A tractable analytic expression for the physics of the effect of the flow shear on the effective classical stability of the total current density profile is presently not available.

Flow shear needs to be put into an analytic expression for Δ' to guide comparisons to experiments. A large aspect ratio circular cylinder asymptotic solution for Δ' (without flow) from Ref. [31] is the basis; this work includes realistic geometry for finite aspect shaped cross sections but, for simplicity, we will use the simpler geometry which was also derived in Ref. [32]. For $m \geq 2$, the tearing index Δ' in this simple geometry is

$$\Delta' = -(2m/r)\,\lambda\pi\cot(\lambda\pi) \quad , \tag{2a}$$

with

$$\lambda = -\frac{rq}{m(dq/dr)}\frac{\mu_0}{B_\theta}\frac{dj_\parallel}{dr} = -\frac{rL_q}{m}\frac{\mu_0}{B_\theta}\frac{dj_\parallel}{dr} \quad , \tag{2b}$$

and L_q defined as the radial magnetic shear length

$$L_q = q/(dq/dr) \tag{2c}$$

where all quantities are evaluated at the rational surface $r = r_s$, the index s being dropped now for simplicity. Here $j_\parallel$ is the total current density parallel to the total magnetic field

which allows for situations where this differs from that of the toroidal current density being dominant. Note that $\Delta' \to -2m/r$ for $\lambda \to 0$, i.e., very stable, and $\Delta' \to 0$ for $\lambda = 1/2$, i.e., marginal classical tearing stability. Further, the usual negative $dj_{\|}/dr$ is destabilizing, i.e., large local current density gradients are destabilizing, and the usually positive radial magnetic shear dq/dr is stabilizing. As noted in Ref. [15], with λ the ratio of two gradients, and $\Delta'(\lambda)$, small variations in profiles can make large variations in Δ', in the absence of rotation. Expanding Eq. (2) in λ, the leading term in the region of interest where $\Delta' < 0$, gives

$$-\Delta' r/2\,\mathrm{m} \approx 1 - (\lambda\pi)^2/3 + \ldots \quad . \tag{3}$$

This goes to zero at $\lambda = 0.552$ instead of 0.500. Scaling λ by 1.10 times makes the expansion of Eq. (3) in very good agreement with the analytic expression as shown in Fig. 9 (curve with label NFS = 0.0). In order to have a tractable analytic expression to compare with experiment, we propose that the effect of the flow shear is modeled by replacing L_q^{-1} in Eq. (2b) with

$$L_q^{-1} \to L_q^{-1} - \left(\frac{q}{r/R}\right)\frac{d\Omega_\phi}{dr}\tau_A \quad . \tag{4}$$

This, as will be seen, produces a simple formula for the direct effect of flow shear on Δ'. The choice here of geometric factor $q/(r/R)$ is essentially B_T/B_θ and yields a normalized flow shear (NFS) that is the product of the radial gradient of the toroidal flow times a "parallel" projection L_s in an island of the radial magnetic shear length L_q. The choice of the Alfvén time τ_A (using B_T instead of B_θ) normalizes the flow shear for ideal MHD field line bending which resistive MHD is really everywhere except at the tearing layer. No explicit free-fitting parameter is included in Eq. (4); however, this will be evaluated when comparing to experiment. $L_s = qL_q/(r/R)$ arises in theory in the parallel connection length along an island of full width w, $\lambda_{\|} = L_s/(k_\theta w/2)$ for $k_\theta = m/r$. This normalized flow shear defined as

NFS = $-(d\Omega_\phi/dr)L_s\tau_A$ was previously used as an indicator of relative flow shear for the onset of $m/n=2/1$ modes [33,34] and for the magnitude of $m/n=3/2$ modes [13], but without an analytic model developed here. Note for the usual co-flow peaked on axis profiles, $-d\Omega_\phi/dr$ is taken as positive.

Combining Eqs. (2), (3) and (4), one gets a working analytic model for Δ' that includes flow shear

$$\frac{\Delta' r}{-2\mathrm{m}} \approx 1-\frac{\pi^2}{3}\frac{(1.10\,\lambda)^2}{(1+NFS)^2} \quad . \tag{5a}$$

$$\frac{\Delta' r}{-2\mathrm{m}} \approx 1-\frac{\pi^2}{3}\frac{(1.10\,\lambda)^2}{\left[1-2\left(d\Omega_\phi/dr\right)L_s\tau_A+\left(d\Omega_\phi/dr\right)^2 L_s^2\tau_A^2\right]} \quad . \tag{5b}$$

The denominator is written in Eq. (5b) in this form to make clear the existence of both linear and square terms in normalized flow shear, which will be discussed. In this model, the usual situation is for flow shear to reduce the effective λ making tearing more stable. Also, flow shear would have little effect for very stable current profiles (λ small) and a large effect for marginally stable current profiles ($1.10\,\lambda \lesssim \sqrt{3}/\pi$). Other model choices could be made.

The effect of flow shear in Δ' is given in Fig. 9 for NFS = 0.0, 0.5 and 1.0. If the shear were added in quadrature instead of linearly [as in Eq. (4)], Eq. (5b) would be the same but without the linear term in the denominator. Adding the shears as in Eq. (4) leaves the possibility of a sign effect in Eq. (5) but this would be eliminated by just considering the magnitudes of the shears in Eq. (4) so that the linear denominator term in Eq. (5b) is a positive definite. In the usual situation, $d\Omega_\phi/dr<0$ so $-(d\Omega_\phi/dr)L_s\tau_A$ is positive. As indicated in Fig. 9, flow shear has a stronger effect on Δ' as marginal classical tearing stability without flow shear is approached, i.e., as the scaled λ is increased to 0.55 (λ/1.10 to

1/2). Anecdotally, it has long been puzzling why NTM behavior, while theoretically depending on minutiae of current and q profiles through Δ', is robust to them. The presence of a significant flow shear obviates such profile details with the flow shear improving stability while not removing all sensitivity to profiles. Thus flow shear here makes stable classical tearing yet more stable and insensitive to profiles, i.e., λ. How much effect flow shear has on the effective classical Δ' in this model depends on how close to marginal the stability is without flow shear.

V. REDUCTION OF BETA FOR NTM ONSET WITH LOWER ROTATION IN DIII-D, NSTX AND JET

Reduced plasma rotation is experimentally found to destabilize NTMs at lower beta in DIII-D [33], NSTX [34] and JET [35]. This would be consistent with the picture described earlier in this paper that reduced plasma rotation makes for less flow shear which causes Δ' to be less negative; thus, the energy needed from the helically perturbed bootstrap current to destabilize the NTM is lowered. Each of the three devices have experiments in high confinement H-mode with periodic edge localized modes (ELMs) and with periodic or occasional $m/n = 1/1$ sawteeth and/or fishbones. Slow ramp ups of beta are made on a time scale longer than the energy confinement time τ_E until instability occurs. The plasma rotation is varied "shot-to-shot" in each device by very different means, to be discussed. Again, we note that the onset mixes the physics of Δ', the small island stabilization effects, and the seeding of the NTM; thus, while a $\beta \propto -\Delta'$ dependency may dominate the onset, other effects of rotation can occur as discussed in Ref. [33].

A. DIII-D

The onset of $m/n = 2/1$ modes in DIII-D is presented in detail in Ref. [33]. Rotation is varied by the mix of co- and counter-beam injection torque. There is a clear onset beta fall with

counter-plasma rotation in DIII-D as shown in Fig. 10(a). This has a remarkably equal correlation with normalized flow shear as shown in Fig. 10(b) as the rotation and safety factor profiles remain essentially the same when transitioning from all co-beams to as far in the counter-beam dominated direction as was possible. Removing the all co-NFS of $\simeq 0.55$ lowers the onset beta by about 37% which would be the relative reduction in $-\Delta'$ if other physics (threshold and seeding) was unchanged. The factor $(1 + \mathrm{NFS})^2$ in Eq. (5) thus decreases from 2.4 to 1.0 and a two-point fit to the model of Fig. 9 yields $\lambda = 0.35$ and $\Delta' r = -2.0$ without flow shear and –3.2 with the all co-beams flow shear. Note that for counter-rotation with the same profile shape as co, the flow shear also reverses sign while the safety factor shear does not. The trend shows beta continuing down with the reversed flow shear suggesting a sign effect or an offset minimum in the counter-direction which has not yet been reached.

B. NSTX

The onset of $m/n = 2/1$ modes in the low aspect ratio NSTX is presented in detail in Ref. [34]. In addition to a considerable range in rotation from the broad data set analyzed, rotation is explicitly varied by application of nonresonant $n = 3$ static magnetic field from an external coil as only co-beams are available; the "bumpy" magnetic field exerts drag on the rotation [36]. The strongest correlation with instability onset is found between "noise-prone" parameters (i.e., gradients) which provides confidence that this is the correct physics. The local mode drive versus rotation at $q = 2$ is shown in Fig. 11(a). This drive uses the full kinetic profile analysis to compute the bootstrap current from the Sauter model [37]. It is noted in Ref. [34] that this is well correlated with the electron only drive proportional to the local electron poloidal beta. However, the data is only poorly correlated in general with rotation in Fig. 11(a). The correlation is much stronger with normalized flow shear as shown

in Fig. 11(b). The slopes of the lines for the different seeding sets are similar within error; this suggests that the physics is likely not related to triggering, but rather the underlying tearing stability. Note that the degeneracy in scaling between Ω_ϕ and $d\Omega_\phi/dr$ found in DIII-D is broken in NSTX so that the improved correlation occurs with $d\Omega_\phi/dr$, not Ω_ϕ. For the ELM trigger cases with the highest correlation of Fig. 11(b), the NFS is up to 1.25 and the fit extrapolates to a 76% reduction in onset beta if the flow shear is reduced to zero (same profiles assumed) and other physics unchanged. The factor $(1 + \mathrm{NFS})^2$ in Eq. (5) decreases from 5.1 to 1.0 and a two-point fit to the model of Fig. 9 yields $\lambda = 0.45$ and $\Delta' r = -0.8$ without flow shear and –3.4 with the largest flow shear. Note that neglecting shaping in the low aspect ratio NSTX pushes this model much further than used in DIII-D and JET.

C. JET

The onset of $m/n = 3/2$ modes is described in part in Ref. [35]. Rotation was varied in two ways: by substituting ion cyclotron resonant heating (ICRH) power with no applied torque for co-neutral beam injection power, or by all co-NBI power only varying the mix of co-beams with different injection angles. The ICRH was phased to avoid large destabilizing (seeding) sawteeth. However, one notes that ICRH can also be used to either destabilize sawteeth (frequent, small amplitude) or stabilize them (infrequent, large amplitude); this has a profound effect on the beta for destabilization of 3/2 modes [35,38]. The use of toroidally propagating ion-cyclotron-resonance waves for sawtooth control also has significance for 3/2 destabilization in all co-NBI or unbalanced NBI [39]. With the ICRH:NBI mix changed, a clear result was obtained here in the normalized beta for $m/n = 3/2$ onset lowered. This is shown in Fig. 12 as diamond points with onset β_N versus initial $m/n = 3/2$ Mirnov frequency. The separate NBI-only injection angle scan has a similar trend but a limited extent in rotation and thus a much lower correlation. The dashed line is an extrapolation from the

region of fitted data. The fit can only be taken as suggestive. Other hidden variables, particularly the sawteeth amplitude and period are probably playing a role in the seeding for onset. The normalized flow shear (from EFIT and CXS similar to CER in DIII-D and CHERS in NSTX) has only been worked out for the largest all co-NBI torque case and is approximately NFS $\approx$ 0.27 at $q = 3/2$. The reduction in onset beta is about 55% without flow shear and the factor $(1 + \text{NFS})^2$ in Eq. (5) goes from 1.6 to 1.0 by removing all the flow shear; a two-point fit to the model of Fig. 9 yields λ = 0.44 and $\Delta' r$ = –1.4 without flow shear and –3.1 with the largest flow shear.

While it is already pointed out that other physics than Δ' can enter into the onset of modes, the analytic model presents values of tearing stable Δ' that are consistent with the usual educated guess used in modeling of $\Delta' r \approx -m$ (–2 for 2/1 and –3 for 3/2). Further, the highest value and range of the normalized flow shear (in NSTX) has the largest range in flow shear effect on onset beta.

VI. EFFECTS OF FLOW SHEAR ON SATURATED TEARING MODES AND THE "MEASUREMENT" OF Δ' IN DIII-D

For slowly evolving or saturated magnetic islands, Δ' can be "measured" from evaluation of the modified Rutherford equation, Eq. (1), with $(\tau_R / r^2)\dot{w} \approx 0$. The helically perturbed bootstrap current is balanced by the assumed negative classical tearing index Δ'. It is again noted this effective classical Δ' is itself a function of island width w, i.e., $\Delta'(w)$ [19,20] so it is this effective classical Δ' that is evaluated from

$$\Delta' r = -\varepsilon^{1/2} r L_q \beta_{\theta e} / \left(L_{pe} w \right) \quad . \tag{6}$$

This uses the MHD reconstruction EFIT, the Mirnov magnetic probe arrays and the Thomson scattering as described in Ref. [13]. Again, it is assumed that once excited and saturated, the

islands are large enough so that the small island physics [w_{marg} term in Eq. (1)] can be neglected. The flow shear is from the CER data of CVI and includes the use of EFIT for L_s etc. and Thomson scattering for τ_A. The leading term in the analytic model Eq. (5) for small values of NFS (<1/2) has the form of $\Delta' r = -C_0 - C_{\rm NFS} \times (-d\Omega_\phi / dr) L_s \tau_A$. C_0 and $C_{\rm NFS}$ are both positive if the effective classical tearing without flow shear is stable and a positive normalized flow shear has a stabilizing effect. It is assumed that the current and safety factor profiles have "profile consistency" as flow shear is varied. Thus, one would expect C_0 to be constant and $C_{\rm NFS}/C_0 = \vartheta(1/2)$, depending in part on how close the plasma is to $C_0 = 0$.

DIII-D experiments were done in two regimes. The first regime is the standard, sawteething, ELMing H-mode with $m/n = 3/2$ modes that eventually results in $m/n = 2/1$ modes at higher beta [13,33]. The second type of plasma operation is the hybrid scenario without sawteeth but with ELMs in which an $m/n = 3/2$ or 4/3 saturated mode is needed to sustain the q-profile with $q(0) > 1$ fairly flat in the core [10,40].

A. *m/n* = 3/2 saturated modes in sawteething plasmas

1. Shot-to-shot scan

Applied torque was varied shot-to-shot by counter-beam mix in ELMing H-mode with $m/n = 3/2$ modes and the beta raised slowly by NBI feedback until $m/n = 2/1$ modes were excited [33]. The amplitude of the $m/n = 3/2$ modes increases with beta but co-torque obviates this; modified Rutherford equation evaluation was made of $m/n = 3/2$ at $m/n = 2/1$ onset [13]. The result of $\Delta' r$ versus NFS is shown in Fig. 13. Other than linear fits are possible and are discussed in Ref. [13]. In this paper, we now have an analytical model to check for the consistency of the fit and model. The fit to the MRE using Eq. (6) yielded $\Delta' r =$ (–1.9 ± 0.4) + (–2.1 ± 1.4) × NFS with a linear correlation of 0.80. A value of NFS ≈ 0.9 ± 0.8 would thus be needed to make Δ' twice as negative. From $C_0 = -1.9 \pm 0.4$, one gets $\lambda =$

0.415 ± 0.021 from Eq. (3) with the 1.10 factor included. To leading expansion order, $4m(1.10\pi\lambda)^2/3 \approx 8.2 \pm 0.9$, which is not in good agreement with $C_{\mathrm{NFS}} = 2.1 \pm 1.4$ even considering the error bars; but no shaping factor is used in the model, i.e., a large aspect ratio circular cylinder "high m" model is fitted to the finite aspect ratio diverted shape and the model is the zero island width Δ' while the measured Δ' includes any effect of finite island width. Shaping acts both to increase the effective minor radius r_{eff} at $q = m/n$ and as a scalar multiplier of λ [31,41].

2. Time evolution during a discharge

As the 3/2 data was taken with rising beta in time so that more co-torque raised the achievable 2/1 stable beta which obviated the effect of 3/2 island width $w \propto \beta$, a new experimental method was run. The NBI beta feedback was set at a lower constant $\beta_N \approx 1.9$ to try to avoid $m/n = 2/1$ modes. The torque from co-/counter-NBI mix was programmed down slowly (in $\approx 8\tau_E$) and back up (in $\approx 8\tau_E$) as far down (and back up) in $m/n = 3/2$ rotation as possible without onset of the 2/1 NTM. Figure 14(a) shows the time dependence of normalized β_N and the applied torque. Figure 14(b) shows the $m/n = 3/2$ Mirnov frequency and twice the plasma rotation at CER channel 5 which is very close to $q = 3/2$ from EFIT at all times in the sweeps. Flow shear from CER channels 6 and 4 that straddle $q = 3/2$ is shown versus time in Fig. 14(c). Note that as plasma rotation in Fig. 14(b) is lowered, flow shear also comes down as expected but goes to zero at $t \approx 3450$ while rotation is still finite; unlike the situation of rotation profile consistency in the data of Fig. 13, here the profile changes. Zero flow shear at the island appears to be a "forbidden state" for the flow shear jumps to an inverted profile; rotation is still co but locally increasing as seen in Fig. 15. Sweeping rotation back up leads to a jump to the normal negative flow shear gradient, i.e., the forbidden state is crossed going the other way. Two other attempts to go yet lower in plasma rotation by lowering the

minimum torque command in the PCS, produced the same sudden reversal in the flow shear and jump up in $n=2$ Mirnov amplitude but $m/n=2/1$ modes occurred before the sweep back up.

There is little change in the $n=2$ Mirnov amplitude shown in Fig. 14(d) as the relatively small initial flow shear is removed. Figure 14(d) also shows how after the flow shear inverts, the Mirnov amplitude jumps up to a higher level. During this phase, the co-rotation is still high enough for the vacuum vessel wall to remain a "perfectly conducting" boundary condition, i.e., $\omega\tau_w \approx 60$ where $\tau_w \approx 2$ ms is the wall time for $m/n=3/2$. The island width (about 6 cm during this phase and 4 cm before and after) is large enough to wash out the small island threshold effects; particularly, note that twice the ion banana width at $q=3/2$ over $\sqrt{3}$ is about 1.6 cm so has no significance in Eq. (1). On sweeping back up in torque, however, the Mirnov amplitude initially remains high and then drops back down leading the flow shear "reversion" from inversion to normal. Note that the ubiquitous jumps (fast down and slow back up) in Mirnov amplitude are correlated with the periodic ELMs, not shown; this is the result of "flux pumping" as described in Ref. [40] and is the effect of the short, transient ELM peeling/ballooning instability to rapidly lower the $m/n=3/2$ mode amplitude, followed with a slower relaxation back up in amplitude. During the low rotation, high $m/n=3/2$ amplitude phase, the $m/n=1/1$ sawteeth have mostly gone away, changing into low amplitude (periodic ~0.5 G) $m/n=1/1$ "flutter" as is observed in hybrid scenario plasmas. EFIT indicates that $q=3/2$ has changed location little. EFIT also indicates the magnetic shear has no significant difference. Thus, the increase in $m/n=3/2$ Mirnov amplitude is a direct measure proportional to both the increase in the magnitude of the helical current sheet at the rational surface and to the square of the island width.

Evaluation of the MRE is shown in Fig. 14(e) for times before, during and after the local flow inversion. Keeping the sign dependence in NFS allows for the effect of the flow shear inversion to make Δ' less negative when flow shear jumps from negative (NFS+) to positive (NFS–). Not used explicitly in the linear fit but added as horizontal lines is the possible alternate interpretation that $\Delta' r$ goes from an average of -1.22 ± 0.08 with monotonically decreasing flow (averaging both during sweep down and sweep up) to -1.04 ± 0.01 with locally increasing flow (inverted). The inverse ratio squared in Δ' is about 1.4 and accounts for most of the jump in $n = 2$ Mirnov amplitude in Fig. 14(d). Of course, the data is neither extensive enough to prove the sign effect (or an offset minimum not yet reached for small negative NFS), nor just a subtle change in Δ' due to small changes in the $j_{\|}$ and q profiles (derivatives actually) when flow shear inverts. The values of NFS shown in Fig. 14 are quite low as reducing the feedback β_N to avoid 2/1 modes, also reduced the initial all co-torque, lowering the initial rotation (before the sweep) and flow shear considerably. Further, perhaps because of the reduced injected beam power and, thus, beam fueling, density is lower and this may then, in turn, be allowing deeper beam penetration which translates into less shear in the core flow. The toroidal rotation profiles are shown in Fig. 15 for times at the peak Mirnov amplitude during local flow inversion and just before the torque sweep (scaled by 0.22 times to overlay). The EFITs give the same $q = 3/2$ location with slightly different uncertainties (from $\pm$ 5% uncertainty in MSE EFIT measure of q). The NFS $\equiv 0$ value found of $\Delta' r$ of -1.1 ± 0.1 for the swept shot is statistically just in disagreement (> one sigma) with the value fitted in Fig. 13 of -1.9 ± 0.4 for the multi-shot data set. The island size for the swept discharge is also at the low range of the multi-shot data set (as lower beta) so the nonlinear correction $\Delta'(w)$ may be less. Subtle changes in $j_{\|}$ and q profiles may explain the difference between shot-to-shot operation and a time evolution, i.e., one has β ramping up with fixed torque (Fig. 13) and the other has torque ramping down and back at fixed β

[Fig. 14(e)]. The limited range of the data for NFS makes for a fitted value of $C_{\rm NFS} = 3.6 \pm 3.0$ which is in agreement within error bars for the multi-shot data set value of 2.1 ± 1.4. Again, an alternate explanation of the experimental behavior that cannot be ruled out is no dependence on flow shear before and after the inversion, with Δ' less negative during the inversion due to slight changes to the $j_{||}$ and q gradient profiles, and/or change in differential flow between $q = 3/2$ and other surfaces, i.e., $q = 2/2$ and 4/2.

B. m/n = 3/2 saturated modes in hybrid scenario plasmas

The predominant situation in the hybrid scenario is a "stationary" plasma with an $m/n = 3/2$ mode, no $m/n = 1/1$ sawteeth, periodic ELMs, beta constant under NBI feedback by the PCS and line averaged density kept constant under "puff and pump", i.e., gas puffing and divertor cryopumping controlled by the PCS. The safety factor on axis $q(0)$ is close to but just above unity and the q-profile in the core is fairly flat. Typically, β_N here is kept to about 10%–20% below the $n = 1$ ideal kink no wall beta limit [42]. However, this could still be enough to somewhat reduce the classical stability of the $m/n = 2/1$ tearing [43,44], a point to be discussed in the data analysis.

With beta and density kept constant at $\beta_N \simeq 2.6$ and $\bar{n} \approx 3.5 \times 10^{13}$ cm^{-3}, an initially stationary hybrid discharge with all co-beams had counter-beams of different levels added to slow plasma rotation. This is the situation discussed in the prologue, Section II. The applied torque, the $m/n = 3/2$ Mirnov frequency and twice the plasma rotation from CER channel 5 are shown in Fig. 16(a)–(c). The lowest rotation case starts to roll over at t = 3750 ms and lock to the wall at t = 3880 ms. As the rotation is lowered, so is the magnitude of the flow shear as shown in Fig. 16(d); the lowest rotation has a small flow shear inversion from t = 3650 ms. As flow and flow shear are reduced, the $m/n = 3/2$ Mirnov amplitude also increases as shown in Fig. 16(e). The major jumps in Mirnov amplitude (at lower rotation)

arise from variations in gas puffing to keep density up, from NBI power transients to keep β up and variations in the applied torque as the beams are adjusted to keep beta constant. The double beam feedback (with up to 6 co- and 2 counter-beams) has a "bang-bang" nature; too high a beta cuts out most beams transiently which also reduces the torque. The Mirnov amplitude drops transiently, but interestingly not at the large co-torque large co-rotation, high flow shear (125469 for example); this is consistent with large flow shear making the tearing stability "stiffer". The minor variations are from periodic ELMs. A total of seven discharges (including two similar to others not shown for clarity in Fig. 16) are analyzed for $\Delta' r$ versus NFS at t = 4075 in Fig. 16(f) except for discharge 125476 at t = 3750 before locking. Again, $\Delta' r$ is "measured" from Eq. (6). The best fit has $\Delta' r = -0.65 \pm 0.05 - (1.8 \pm 0.5) \times$ NFS. Note the less negative $\Delta' r$ *without* flow shear in the hybrid (–0.65 ± 0.05) than found in the sawteething plasmas (–1.1 ± 0.1 by time evolution or –1.9 ± 0.4 by shot to shot) may be due to the reduced magnetic shear at $q = 3/2$ in the hybrid with flatter core q-profiles and/or due to the higher beta closer to the $n = 1$ kink limit. The value of normalized flow shear to make $\Delta' r$ twice as negative is NFS = 0.36 ± 0.13. For $\Delta' r = -0.65 \pm 0.05$ at NFS = 0, $\lambda \approx$ 0.47 [again from Eq. (3)] with negligible uncertainty from the model (noting yet again that the model has no shaping and adding that the hybrid plasma is more strongly shaped than the sawteething plasmas). From $\lambda \approx 0.47$, $4\mathrm{m}(1.10\,\pi\lambda)^2/3 \approx$ 10.6 which is (again as in Section VI.A.1) <u>not</u> in good agreement with the fitted $C_{\mathrm{NFS}} = 1.8 \pm 0.5$. The model without shaping is consistently overestimating for $m/n = 3/2$ in both regimes studied. The larger elongation and triangularity of the q = 3/2 surface in these hybrid upper balanced double-null divertor shapes could be making the disagreement larger than in the lower single-null divertor less strongly shaped "ITER" configuration analyzed in Section VI.A.

For 125476, the three times analyzed by PEST-3 in Table I, were also analyzed by the MRE balance method. Only the lowest rotation time (3750) is included in the multi-shot fit of Fig. 16. The values of $\Delta' r$ are found to be –1.03, –0.81 and –0.65 at t = 3425, 3665 and 3850 ms, respectively. The linear temporal fit with NFS is $\Delta' r$ = –0.70 – 1.48 × NFS, linear correlation of –0.97, and is in good agreement with the multi-shot single time fit of Fig. 16 of $\Delta' r$ = –0.65 ± 0.05 – (1.81 ± 0.46) × NFS, corr = –0.93. The MRE extracted values of $\Delta' r$ can now be compared with the PEST-3 values of $\Delta' \psi_s^{2\mu}$ in Table I. The systematic effect of flow shear on the effective classical tearing stability is well captured by the MRE method and is, of course, not included in PEST-3.

VII. SIGN DEPENDENCE OR OFFSET IN FLOW SHEAR EFFECT ON Δ' ?

DIII-D experiments went as far in the counter-direction as possible (normal I_p with 2 of 7 beams counter or reversed I_p with 5 of 7 counter available) but loss of ELMing H-mode with counter-domination limited the counter-scan. The trend for 2/1 onset in beta (Fig. 10) or 3/2 saturated mode $\Delta' r$ (Fig. 13) continued down as counter-rotation magnitude increased. Counter-rotation with peaked on axis amplitude has a positive flow shear compared to co-rotation peaked on axis which has a negative flow shear. Plasmas with co-rotation but inverted (hollow) local flow at the $q = 3/2$ surface also have positive flow shear and the 3/2 mode amplitude increased (Fig. 14). The diagrams shown in Fig. 8 would have an additive effect of shears for the usual co-flow and particles going parallel to $\dot{B}$ with a subtractive effect for counter-flow or co-flow inverted. However, there is no published result of the physics for the "sign" effect of flow shear (with positive magnetic shear), i.e., that negative flow shear is stabilizing while positive flow shear is destabilizing. Until definitive experiments are performed, either counter-dominated flow with same ELMing, H-mode or off-axis NBI to controllably vary (invert) flow profile (DIII-D in 2011), one can speculate that

rather than a sign effect, there is an offset "zero" in flow shear not yet reached in the counter-direction.

Because of inertial and viscous effects, once an island forms, even at small size, the different response of the electrons and ions tend to make the island propagate in the lab frame faster in the co-direction than the plasma [23,45]. Here the relevant plasma flow is $E\times B$ which makes the local radial electric field E_r zero, i.e., $E\times B = 0$ in a frame going at this rotation; this is usually dominated by toroidal rotation and is identically the same for electrons, main ions, and any impurity ions. The island flow in the lab frame is thus, if viscosity dominates, $\Omega_{\phi,lab} \approx n\Omega_{\phi i} + \Omega_i^*$ where $\Omega_{\phi i}$ is the toroidal plasma flow angular frequency (from CER of CVI for example as here on DIII-D) and Ω_i^* is the ion diamagnetic drift frequency in the co-direction for the usual profiles and directions. Thus a zero value of $\Omega_{\phi i}$ would still leave a non-zero co-value Ω_i^* and a true offset null flow is in the counter-direction at $\Omega_{\phi i} \approx -\Omega_i^*$. Now $\Omega_i^* = nk_B T_i (dp_i/d\psi)/ep_i$ for mode m/n where p_i is the ion pressure and ψ is the poloidal flux (which constitutes a "radial" coordinate) [23]. Thus, depending on the ion pressure and temperature profiles, the shear in Ω_i^* can have a different radial profile than the shear in $\Omega_{\phi i}$, and the sum of the shears can, in turn, change sign, particularly at low values of $\Omega_{\phi i}$. Flow shear is modified with this effect as

$$\frac{d\Omega_{\phi i}}{dr} \rightarrow \frac{d\Omega_{\phi i}}{dr} - \frac{\Omega_i^*}{nL_{Ti}}\left[1 - \frac{L_{Ti}\,p_i}{dp_i/d\psi} \times \frac{d}{dr}\left(\frac{dp_i/d\psi}{p_i}\right)\right] \tag{7}$$

For counter-toroidal flow with monotonically decreasing amplitude towards the boundary, $d\Omega_{\phi i}/dr$ is positive and is of opposite sign to co-toroidal flow peaked on axis. The ion temperature gradient term dominates the shear in the ion drift frequency which is itself "always" in the co-direction; $L_{Ti} \equiv -T_i/dT_i/dr > 0$ for peaked ion temperature profile. Thus the second term in Eq. (7) is "always" negative. Note that the profile correction from the

bracket is essentially a gradient of a gradient and problematic to evaluate. The bracket in Eq. (7) is found to be about one for the discharge to be analyzed. Thus a null in the "island flow shear" may occur at a value of positive toroidal rotation shear (peaked counter or hollow co); this is a negative value of the normalized flow shear as defined in this paper.

For DIII-D discharge 126681 at $m/n = 2/1$ onset with normal I_p and both counter-beams fully on (and only one co-beam on for 10 ms in every 30 ms interval), $\Omega_{\phi i}/2\pi$ = –2.5 kHz from CVI CER and $\Omega_i^*/2\pi$ using CVI CER is +1.1 kHz. The toroidal flow shear $d\Omega_{\phi i}/dr$ is +35 krad/s/m, i.e., positive as the negative $\Omega_{\phi i}$ is peaked on axis. Taking $(dp_i/d\psi)/p_i$ as about constant within uncertainty, the shear in Ω_i^* comes from the gradient in T_i and $d\Omega_i^*/dr$ is –23 krad/s/m. One expects the null in the shear in $\Omega_{\phi i} + \Omega_i^*$ has already just been passed in this case; the null in the island flow shear is in the net counter-torque direction. Note we have neglected both the poloidal rotation and ∇p_i terms in the $E \times B = 0$ frame in which rotation would be at Ω_i^*. Further, we have used CVI CER rather than a diagnostic for the main deuterium ions which are expected to rotate a little faster in the co-direction [12] (but have similar shear). More definitive deeper counter-rotation data is needed to resolve a minimum from a true-sign effect.

VIII. CONCLUSIONS AND FUTURE WORK

Reducing plasma rotation has the causal effect of lowering the beta at which tearing modes are destabilized and/or making pre-existing tearing modes larger in amplitude. In general, local flow shear is at least as well if not better correlated with the effects as the plasma flow (rotation). Subtle effects of plasma rotation on the intrinsic plasma current profile tearing stability may play a role but have not been identifiable. For onset of tearing, the effects of

plasma rotation on seeding and small island thresholds are also yet to be shown. For existing "large" tearing modes, however, such seeding and threshold effects should be inoperative.

A level for significant tearing stabilizing plasma rotation (flow) radial shear is found of $-d\Omega_\phi/dr \approx \vartheta(\tau_A^{-1}/2L_s)$ at rational surface $q = m/n$. This is interpreted to have a substantial stabilizing effect on the effective classical tearing Δ'; removing it makes $-\Delta'$ less negative, i.e., less stabilizing. Thus, there is an advantage for all co-neutral beam heated plasmas with strong torque driving rotation. An ad hoc analytic way in which flow shear enters into Δ' is proposed; in this model, otherwise large temporal variations in Δ' due to small changes in the equilibrium current and safety factor profiles are obviated as the flow shear removes sensitivity to "bad" gradients in the current density. Results show near zero rotation plasmas are much less stable than a simple $\Delta' r$ = –2 m or even –m model frequently used for analysis and modeling.

Some of the experimental data suggests (or hints at) a destabilizing effect of "inverted" flow shear exists. A counter-direction offset in the null for flow shear may not yet have been reached and thus may be mimicking a sign effect. A new tool of off-axis NBI is planned for DIII-D in 2011 which could allow controlled inversion of the rotation profile [46].

Numerical modeling in realistic geometry for finite aspect ratio shaped tokamak equilibria is in process with the NIMROD [47] and MARS [48] codes to better understand the flow and flow shear effects on tearing stability. The NIMROD code solves the linear and nonlinear MHD equations as initial value computations, optionally including numerous effects such as equilibrium flow and multiple fluid species within the MHD treatment. MARS solves the linearized resistive MHD equations to calculate eigenvalues and eigenvectors for individual unstable toroidal modes also including several physical effects outside of the conventional

MHD treatment. Results from numerical modeling from these codes are expected to be reported in future papers.

ACKNOWLEDGMENT

The authors are grateful for discussions and support from Ming Chu, Craig Petty, Peter Politzer and Ted Strait of General Atomics, D. Raju and A. Sen of the Institute of Plasma Research-Gujarat, Chris Hegna of the University of Wisconsin-Madison, Scott Kruger of the Tech-X Corp., Francois Waelbroeck of IFS-Austin, and, of course, the DIII-D, NSTX and JET Experimental Teams.

This work supported in part by the U.S. Department of Energy under DE-FC02-04ER54698 and DE-AC02-09CH11466.

REFERENCES

[1]. R.J. La Haye, Phys. Plasmas **13**, 05501 (2006).

[2]. Z. Chang and J. D. Callen, Nucl. Fusion **30**, 219 (1990).

[3]. M.F. F. Nave and J. A. Wesson, Nucl. Fusion **30**, 2575 (1990).

[4]. C.C. Hegna, J. D. Callen and R. J. La Haye, Phys. Plasmas **6**, 130 (1999).

[5]. F.L. Waelbroeck, J.W. Connor and H.R. Wilson, Phys. Rev. Lett. **87**, 215003 (2001).

[6]. R.J. La Haye, R.J. Buttery, S. Guenter, G.T.A. Huysmans, M. Maraschek and H.R. Wilson, Phys. Plasmas **7**, 3349 (2000).

[7]. J.L. Luxon, Nucl. Fusion **42**, 614 (2002).

[8]. M. Ono, S.M. Kaye, Y.-K. M. Peng, G. Barnes, W. Blanchard, M.D. Carter, J. Chrzanowski, L. Dudek, R. Ewig, D. Gates, R.E. Hatcher, T. Jarboe, S.C. Jardin, D. Johnson, R. Kaita, M. Kalish, C.E. Kessel, H.W. Kugel, R. Maingi, R. Majeski, J. Manickam, B. McCormack, J. Menard, D. Mueller, B.A. Nelson, B.E. Nelson, C. Neumeyer, G. Oliaro, F. Paoletti, R. Parsells, E. Perry, N. Pomphrey, S. Ramakrishnan, R. Raman, G. Rewoldt, J. Robinson, A.L. Roquemore, P. Ryan, S. Sabbagh, D. Swain, E.J. Synakowski, M. Viola, M. Williams, J.R. Wilson and NSTX Team, Nucl. Fusion **40**, 557 (2000).

[9]. M. Keilhacker and the JET Team, Plasma Phys. Control. Fusion **41**, B1 (1999).

[10]. P. A. Politzer, C.C. Petty, R.J. Jayakumar, T.C. Luce, M.R. Wade, J.C. DeBoo, J.R. Ferron, P. Gohil, C.T. Holcomb, A.W. Hyatt, J. Kinsey, R.J. La Haye, M.A. Makowski and T.W. Petrie, Nucl. Fusion **48**, 075001 (2008).

[11]. B. Rice, D.G. Nilson, K.H. Burrell and L.L. Lao, Rev. Sci. Instrum. **70**, 815 (1999).

[12]. W.M. Solomon, K.H. Burrell, R. Andre, L.R. Baylor, R. Budny, P. Gohil, R.J. Groebner, C. T. Holcomb, W.A. Houlberg and M.R. Wade, Phys. Plasmas **13**, 056616 (2006).

[13]. R.J. La Haye and R.J. Buttery, Phys. Plasmas **16**, 022107 (2009).

[14]. H.E. St. John, T.S. Taylor and Y.R. Lin-Liu, in *Proc. 15th Int. Conf. on Plasma Physics and Controlled Nuclear Fusion Research*, Seville, Spain, 1994 [International Atomic Energy Agency, Vienna, 1995) vol. 3, p. 603.

[15]. C.M. Bishop, J.W. Connor, R.J. Hastie and S.C. Cowley, Plasma Phys. Control. Fusion **33**, 389 (1991).

[16]. A. Pletzer, A. Bondeson and R. L. Dewar, J. Comput. **115**, 530 (1994).

[17]. P.H. Rutherford, Phys. Fluids **16**, 1903 (1973).

[18]. M.S. Chu, R.J. La Haye, M.E. Austin, L.L. Lao, E. A. Lazarus, A. Pletzer, C. Ren, E.J. Strait, T. S. Taylor and F. L. Waelbroeck, Phys. Plasmas **9**, 4584 (2002).

[19]. R.B. White, D.A. Monticello, M.N. Rosenbluth and B.V. Waddell, Phys. Fluids **20**, 800 (1977).

[20]. B. Carreras, B.V. Waddell and H.R. Hicks, Nucl. Fusion **19**, 1423 (1979).

[21]. A. Pletzer, "Numerical Δ' Studies of the Nonlinear Finite-β Tearing Mode," eds. J.W. Connor, E. Sindoni, J. Vaclavik, Proc. Joint Varenna-Lausanne Intl. Workshop on Theory of Fusion Plasmas, Varenna, Italy, 1996 (Compositori 1997) pp. 37–45.

[22]. W.X. Qu and J.D. Callen, "Nonlinear Growth of a Single Neoclassical MHD Tearing Mode in a Tokamak," University of Wisconsin Report UWPR 85-5, October 1985.

[23]. R.J. La Haye, C.C. Petty, E.J. Strait, F.L. Waelbroeck and H.R. Wilson, Phys. Plasmas **10**, 3644 (2003).

[24]. A. Kallenbach, H.M. Mayer, G. Fussmann, V. Mertens, U. Stroth, O. Vollmer and The ASDEX Team, Plasma Phys. Control. Fusion **33**, 595 (1991).
[25]. X.L. Chen and P. J. Morrison, Phys. Fluids B **2**, 495 (1990).
[26]. L. Ofman, X.L. Chen, P.J. Morrison and R.S. Steinolfson, Phys. Fluids B **3**, 1364 (1991).
[27]. L. Ofman, P.J. Morrison and R.S. Steinolfson, Phys. Fluids B **5**, 376, (1993).
[28]. D. Chandra, A. Sen, P. Kaw, M.P. Bora and S. Kruger, Nucl. Fusion **45**, 524 (2005).
[29]. R. Coelho and E. Lazzaro, Phys. Plasmas **14**, 012101 (2007).
[30]. C. Ren, M.S. Chu and J.D. Callen, Phys. Plasmas **6**, 1203 (1999).
[31]. C.C. Hegna and J.D. Callen, Phys. Plasmas **1**, 2308 (1994).
[32]. H.R. Strauss, Phys. Fluids **24**, 2004 (1981).
[33]. R.J. Buttery, R.J. La Haye, P. Gohil, G. L. Jackson, H. Reimerdes, E.J. Strait, and the DIII-D Team, Phys. Plasmas **15**, 056115 (2008).
[34]. S.P. Gerhardt, D.P. Brennan, R. Buttery, R.J. La Haye, S. Sabbagh, E. Strait, M. Bell, R. Bell, E. Fredrickson, D. Gates, B. LeBlanc, J. Menard, D. Stutman, K. Tritz and H. Yuh, Nucl. Fusion **49**, 032003 (2009).
[35]. R.J. Buttery, S. Gerhardt, A. Isayama, R.J. La Haye, E.J. Strait, D.P. Brennan, P. Buratti, D. Chandra, S. Coda, J. deGrassie, P. Gohil, M. Gryaznevich, J. Hobirk, C. Holcomb, D.F. Howell, G. Jackson, M. Maraschek, A. Polevoi, H. Reimerdes, D. Raju, S. A. Sabbagh, S. Saarelma, M. Schaffer, A. Sen, JET-EFDA contributors, the DIII-D, JT-60 and NSTX teams, in *Proc. 22nd IAEA Fusion Energy Conf.*, Geneva, Switzerland, 2008 ([International Atomic Energy Agency, Vienna, 2003) IT/P6-8, http://www-pub.iaea.org/MTCD/ Meetings/FEC2008/ it_p6-8.pdf
[36]. R.J. La Haye, S.Günter, D.A. Humphreys, J. Lohr, T.C. Luce, M.E. Maraschek, C.C. Petty, R. Prater, J.T. Scoville, and E.J. Strait, Phys. Plasmas **9**, 2051 (2002).
[37]. O. Sauter, C. Angioni, and Y.R. Lin-Liu, Phys. Plasmas **6**, 2834 (1999).
[38]. O. Sauter, E. Westerhof, M.L. Mayoral, B. Alper, P.A. Belo, R.J. Buttery, A. Gondhalekar, T. Hellsten, T.C. Hender, D.F. Howell, T. Johnson, P. Lamalle, M.J. Mantsinen, F. Milani, M.F. F. Nave, F. Nguyen, A.L. Pecquet, S.D. Pinches, S. Podda, and J. Rapp, Phys. Rev. Lett. **88**, 105001 (2002).
[39]. J.P. Graves, I. Chapman, S. Coda, L.-G. Eriksson and T. Johnson, Phys. Rev. Lett. **102**, 065005 (2009).
[40]. C.C. Petty, M. E. Austin, C.T. Holcomb, R.J. Jayakumar, R.J. La Haye, T.C. Luce, M.A. Makowski, P.A. Politzer and M.R. Wade, Phys. Rev. Lett. **102**, 045005 (2009).
[41]. T.A. Gianakon, C.C. Hegna and J.D. Callen, Phys. Plasmas **3**, 4637 (1996).
[42]. R.J. La Haye, P.A. Politzer and D.P. Brennan, Nucl. Fusion **48**, 015005 (2008).
[43]. D.P. Brennan, E.J. Strait, A.D. Turnbull, M.S. Chu, R.J. La Haye, T.C. Luce, T.S. Taylor, S. Kruger, A. Pletzer, Phys. Plasmas **9**, 2998†(2002).
[44]. D.P. Brennan, R.J. La Haye, A.D. Turnbull, M.S. Chu, T.H. Jensen, L.L. Lao, T.C. Luce, P.A. Politzer, E.J. Strait, S.E. Kruger and D.D. Schnack, Phys. Plasmas **10**, 1643†(2003).
[45]. F.L. Waelbroeck, R. Fitzpatrick and D. Grasso, Phys. Plasmas **14**, 022302 (2007).
[46]. M. Murakami, J.M. Park, C.C. Petty, T.C. Luce, W.W. Heidbrink, T.H. Osborne, R. Prater, M.R. Wade, P.M. Anderson, M.E. Austin, N.H. Brooks, R.V. Budny, C.D. Challis, J.C. DeBoo, J.S. deGrassie, J.R. Ferron, P. Gohil, J. Hobirk, C.T. Holcomb, E.M. Hollmann, R.M. Hong,

A.W. Hyatt, J. Lohr, M.J. Lanctot, M.A. Makowski, D.C. McCune, P.A. Politzer, J.T. Scoville, H.E. St. John, T. Suzuki, T.S. Taylor, W.P. West, E.A. Unterberg, M.A. Van Zeeland and J. H. Yu, Nucl. Fusion **49**, 065031 (2009).

[47]. C.R. Sovinec, A.H. Glasser, T.A. Gianakon, D.C. Barnes, R.A. Nebel, S.E. Kruger, D.D. Schnack, S.J. Plimpton, A. Tarditi, M.S. Chu, the NIMROD Team, J. Comp. Phys. **195**, 355 (2004).

[48]. M.S. Chu, J.M. Green, T.H. Jensen, R.L. Miller, A. Bondeson, R.W. Johnson and M.E. Mauel, Phys. Plasmas **2**, 2236 (1995).

t (ms)	f (kHz)	(G)		(A/cm^2)	
3425	37.0	4.0	1.13	16.4	–0.68
3665	8.6	7.0	1.10	19.1	–0.66
3850	2.0	9.7	0.99	13.0	–0.21

Table I. Linear m/n = 3/2 Δ′ calculations by PEST-3 for discharge 125476 for high, intermediate and low rotation times. MIRNOV analysis and the global beta poloidal and local bootstrap current are also given.

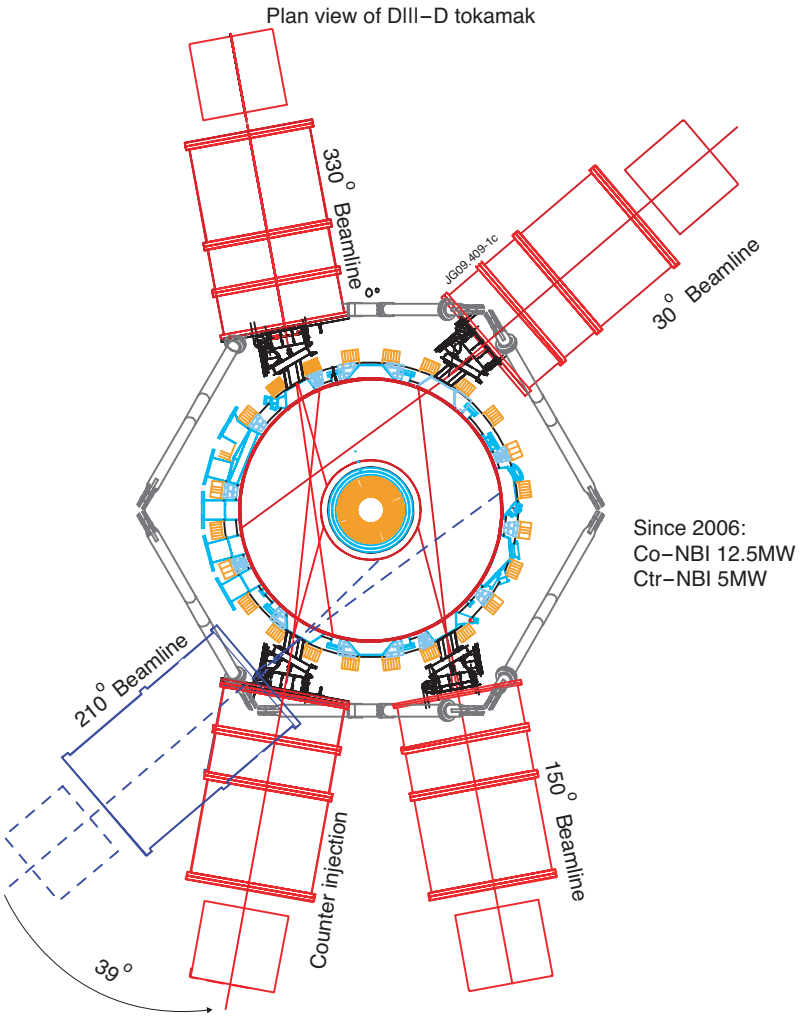

Figure 1: In 2006, one pair of DIII-D beams was moved from co to counter. All near tangential injection. (Adapted from Gohil P 2009 Nucl Fusion 49, 115004. Copyright 2009, IAEA Vienna.)

Figure 2:(a) Applied torque in units (2.4 N-m) of the most co-beam (30 LEFT) in DIII-D and $\beta_N = \beta(\%)/(I/aB)$ (b) m/n = 3/2 and 2/1 Mirnov frequencies, (3) 3/2 and 2/1 Mirnov amplitudes.

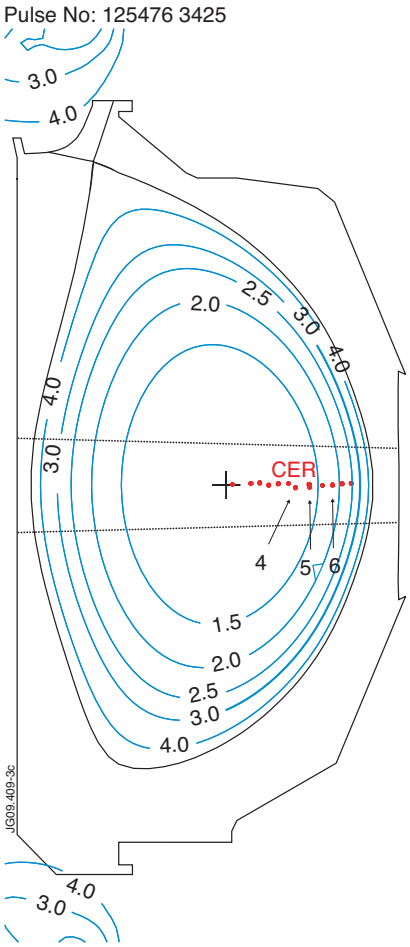

Figure 3: Cross section of DIII-D discharge 125476 at 3425 ms with locations of rational surfaces; m/n = 3/2 is highlighted. Chords 1 to 10 of CER are noted.

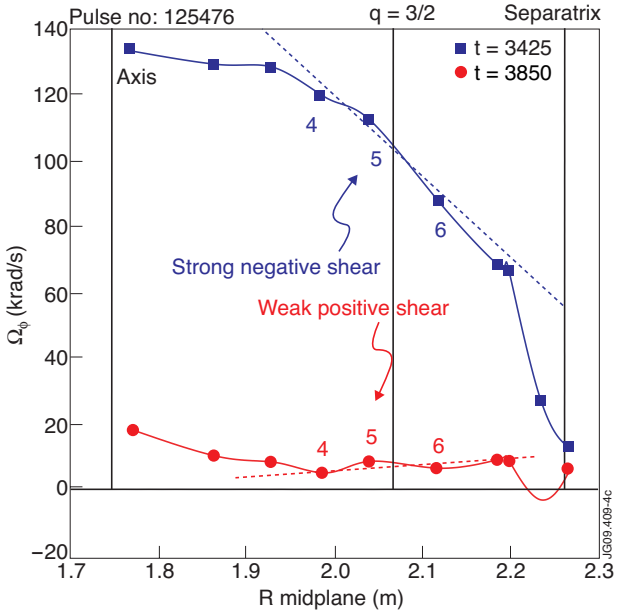

Figure 4: Profiles of toroidal rotation Ω_ϕ versus major radius R in DIII-D discharge 125476 with all co-beams (3425) and near balanced beams (3850). Channels 4, 5, and 6 are noted with number 5 closest to q = 3/2 and numbers 4 and 6 straddling q = 3/2.

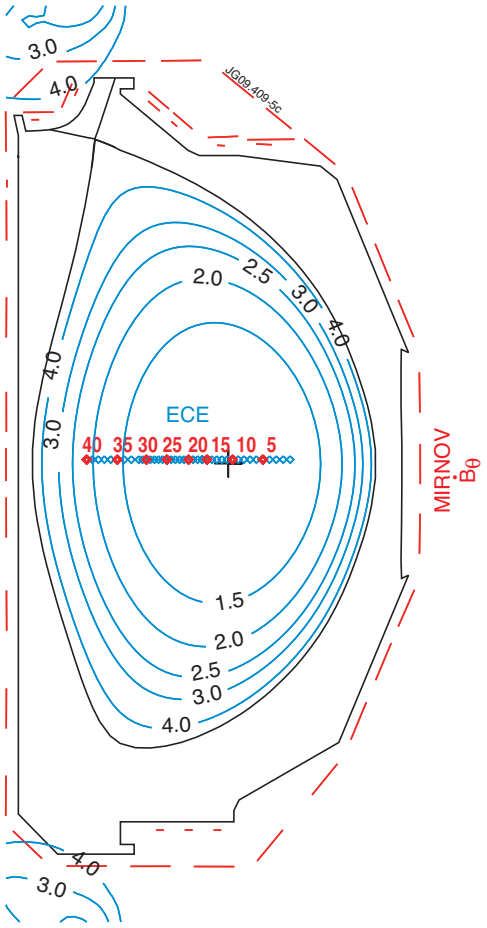

Figure 5: Mode m/n analysis comes from the toroidal and poloidal Mirnov probe arrays in DIII-D. (The short straight segments represent the Mirnov probes that measure $\tilde{B}_\theta$, i.e. the magnetic field parallel to the segments.) Island width analysis from Mirnov and EFIT can be calibrated by the ECE radial profile of perturbed T_e depending on the value of the axial toroidal field B_T and on the plasma electron density being below cutoff.

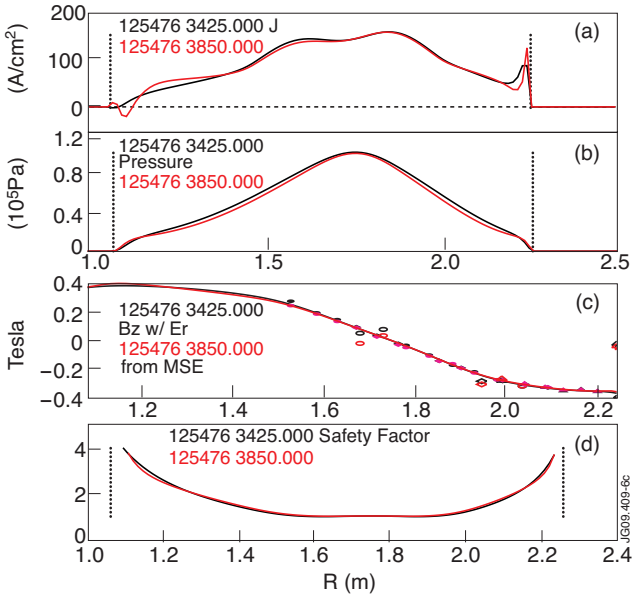

Figure 6: Kinetic EFIT profiles for DIII-D Shot 125476 at t = 3425 and 3850ms. (a) Total current density J, (b) pressure, (c) poloidal field from MSE, (d) safety factor q.

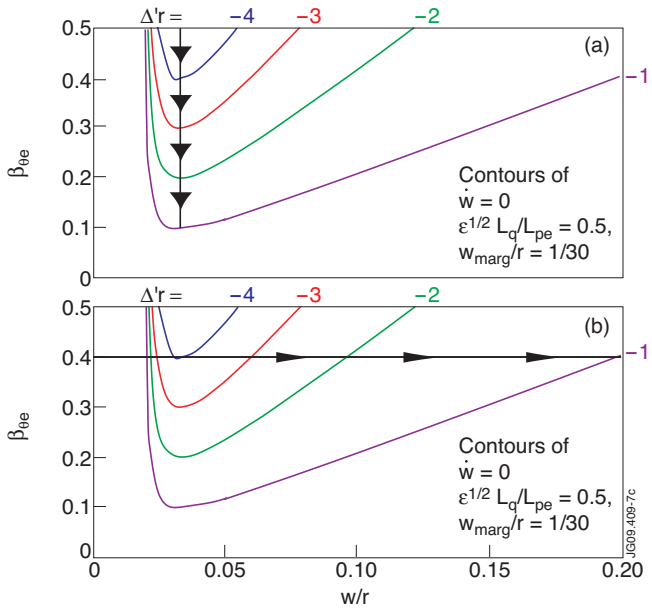

Figure 7: (a) Contours of $\dot{w} = 0$ for β_{θ_e} versus w/r for different values of $\Delta' r$. $\dot{w} > 0$ above each curve and $\dot{w} < 0$ below each curve. The arrows indicate how less negative $\Delta' r$ (less stable) lowers the minimum beta needed to destabilize an NTM (knee of curves). (b) Same contours as in (a), but arrows now show how at fixed beta (here $\beta_{\theta_e} = 0.4$), making Δ' less negative (less stable) increases the size of a saturated island. For $\Delta' r = -4$, the island would self-stabilize at $w = w_{marg}$, i.e., all values of have $w \leq 0$ at $\beta_{\theta_e} \equiv 0.4$.

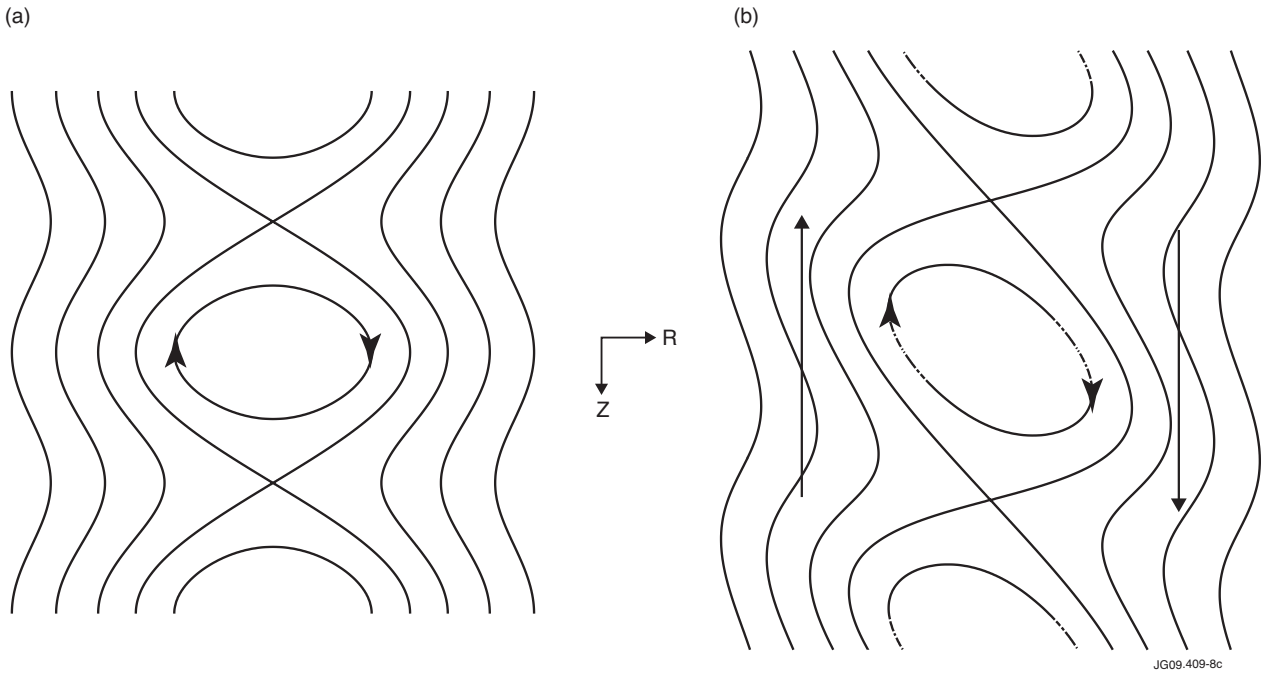

*Figure 8: (a) Island with magnetic shear only with increasing with major radius R (for $R > R_0$) and Z the toroidal direction. Arrows indicate direction parallel to the magnetic field in a frame q = m/n with usual direction in DIII-D of I_p opposite toroidally to B_T. (b) Flow shear added (big arrows) with frame of zero flow at island O-point and flow (co to I_p) decreasing in . (Adapted from La Haye R J 2009 Phys. Plasmas **16** 022107. Copyright 2009, American Institute of Physics.)*

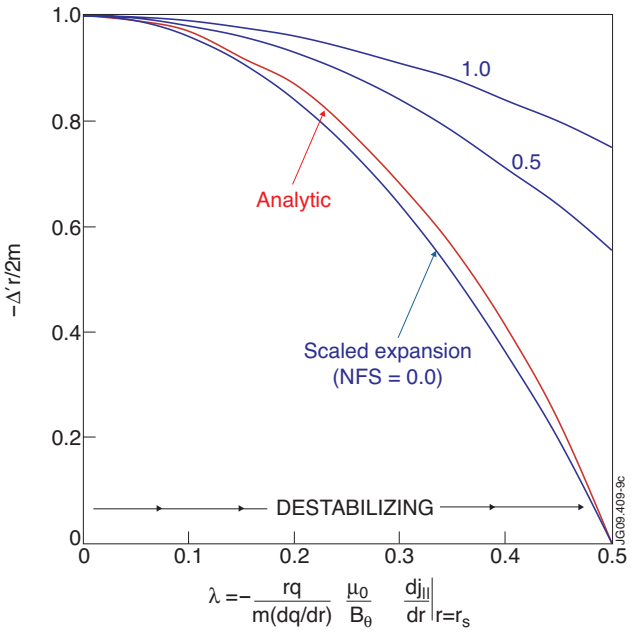

Figure 9: Large aspect ratio circular cylinder analytic expression for Δ′ with comparison to scaled expression (λ×1.10) for normalized flow shear (NFS) of 0.0, 0.5 and 1.0.

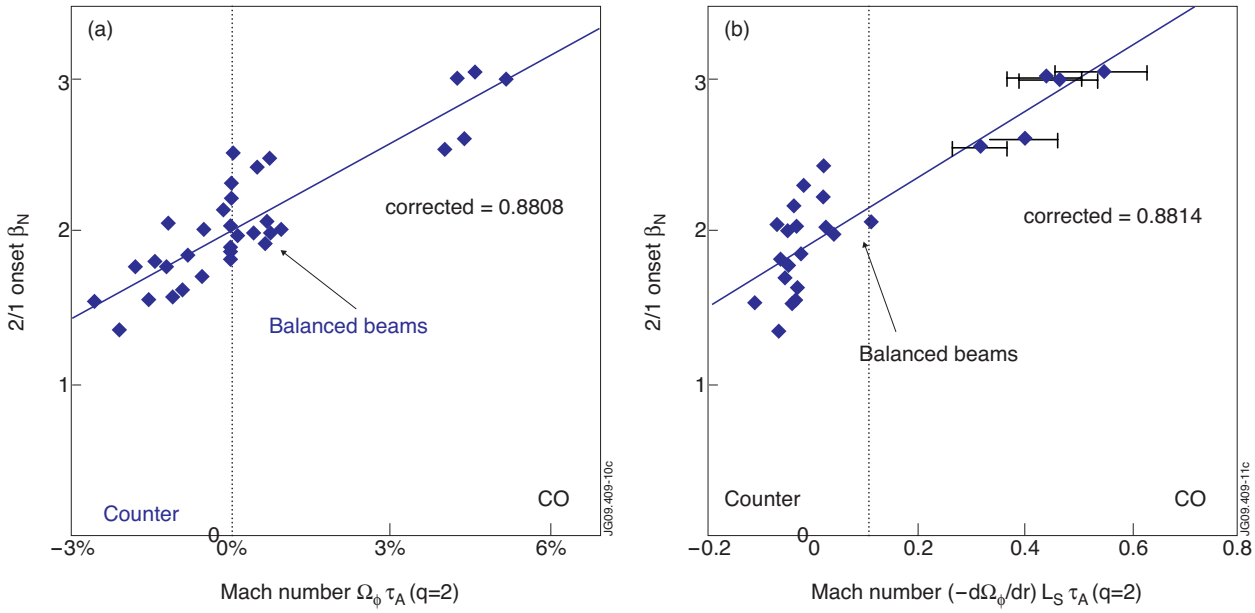

Figure 10: (a) DIII-D m/n = 2/1onset normalized beta with local plasma rotation at q = 2 normalized by Alfvén time for the Alfvénic "Mach Number", (b) same as (a) but versus local normalized flow shear (NFS)."

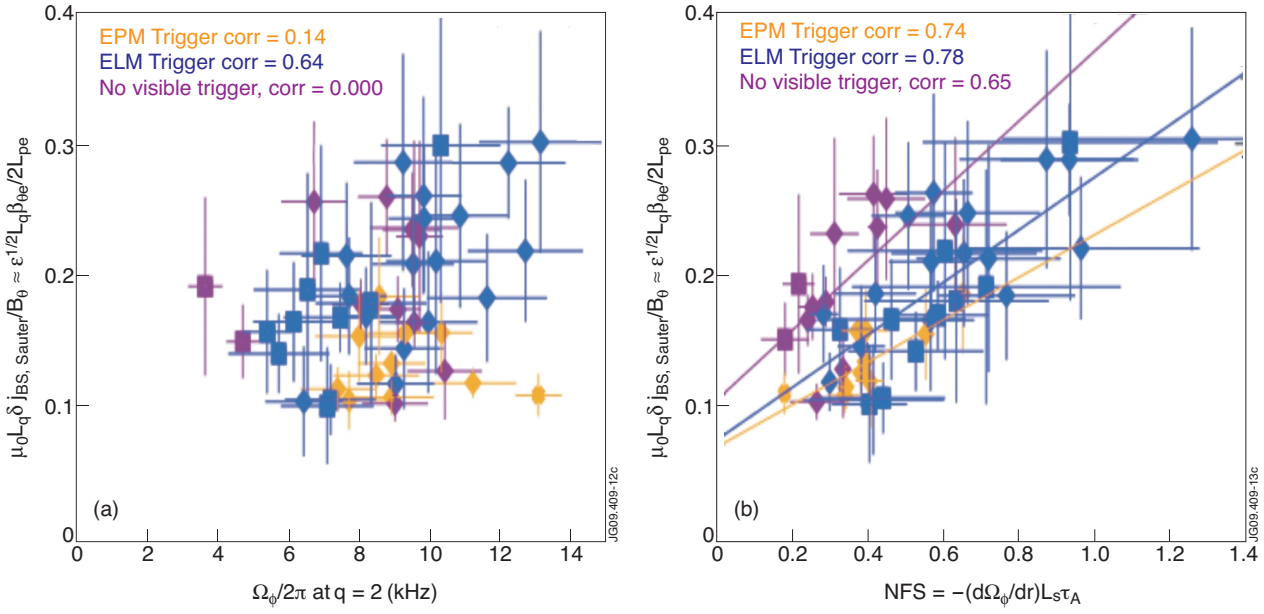

*Figure 11: (a) NSTX m/n = 2/1 onset local mode drive versus plasma rotation at q = 2 with energetic particle mode, edge localized mode or no visible triggers, (b) same as (a) but versus normalized flow shear at q = 2. (Adapted from Gerhardt S P 2009 Nucl Fusion **49** 032003. Copyright 2009, IAEA Vienna.)*

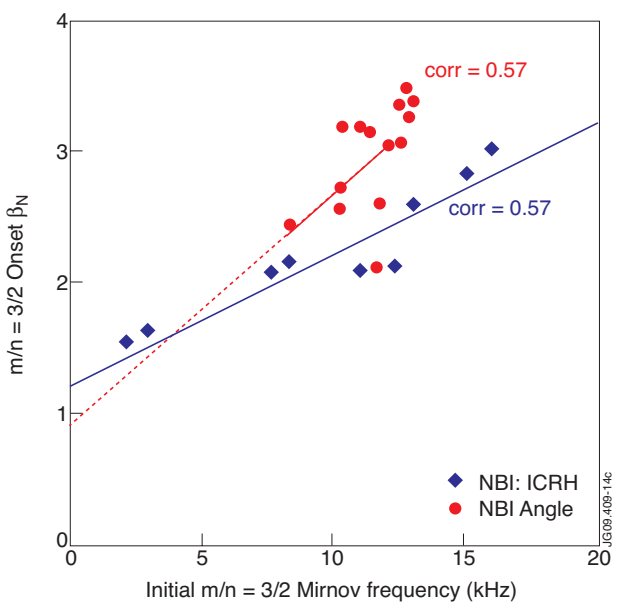

Figure 12:JET m/n = 3/3 onset normalized beta versus initial 3/2 Mirnov frequency. Diamonds (purple) are for data set with NBI and ICRH mixed to vary rotation. Circles (red) are for co-NBI only with different beam angles (to tangency, i.e., near tangential and not as near tangential) to vary rotation.

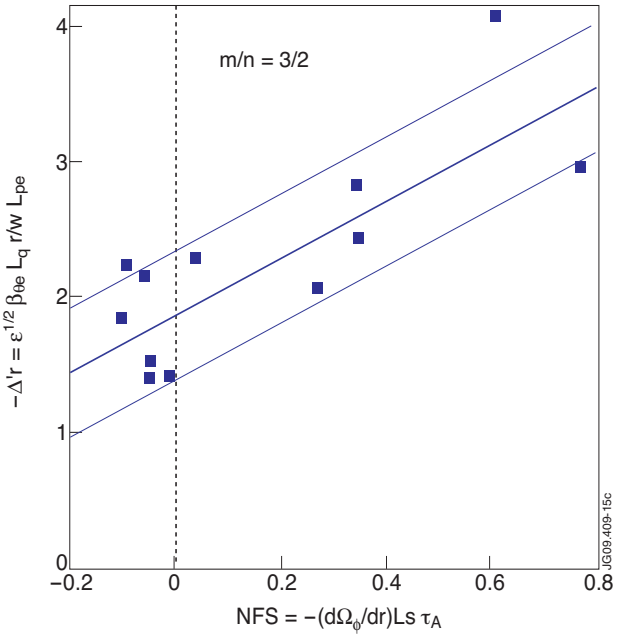

Figure 13: The value of $-\Delta' r$ in DIII-D for m/n = 3/2 inferred from the helically perturbed bootstrap term in the MRE plotted against the normalized flow shear. Correlation of linear fit is 0.80 with σ = 0.48 noted. (Adapted from La Haye R J 2009 Phys. Plasmas 16 022107. Copyright 2009, American Institute of Physics.)

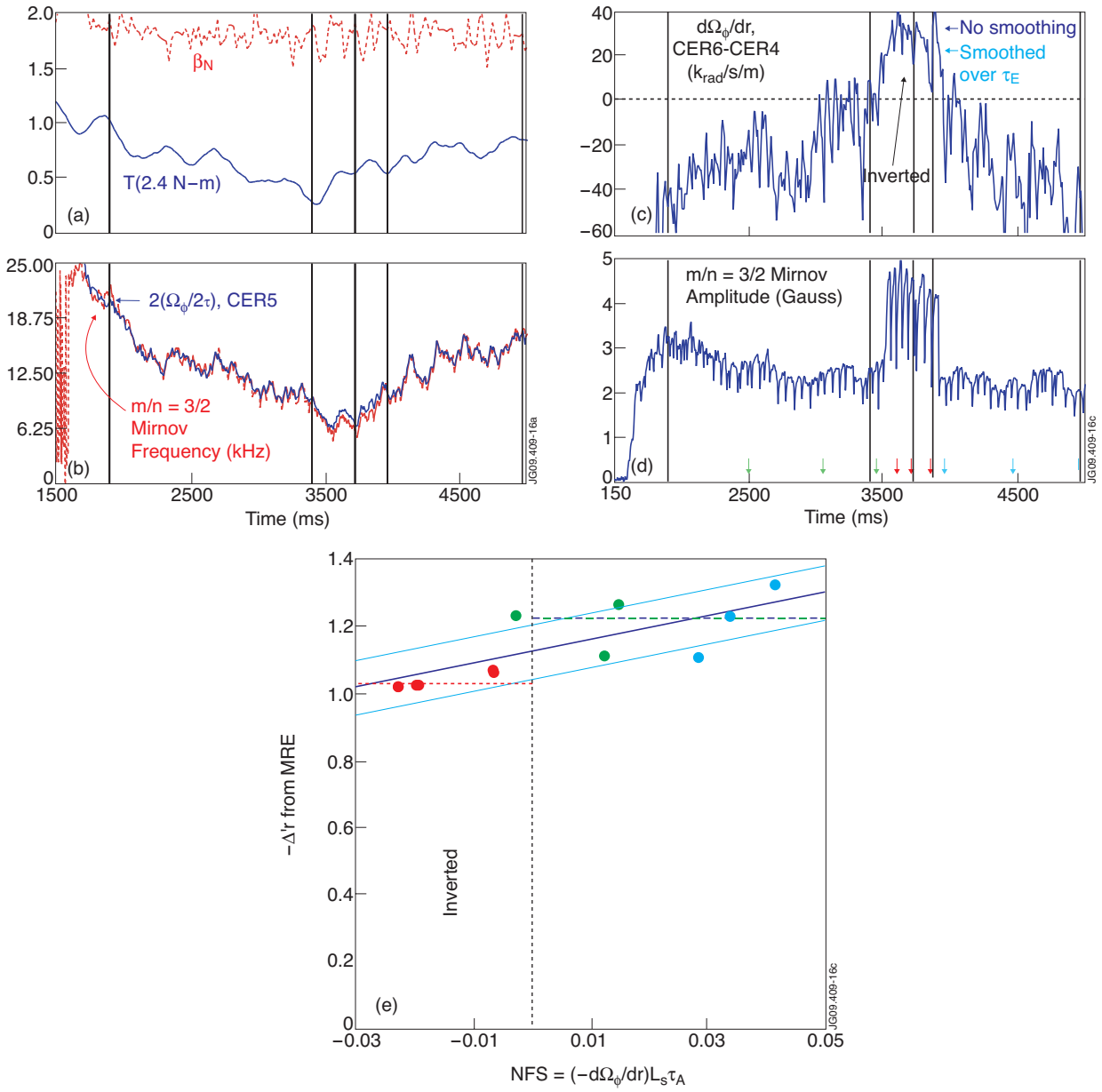

Figure 14: (a) Normalized beta and applied torque versus time in DIII-D discharge 135867. (b) m/n = 3/2 Mirnov frequency and twice the plasma rotation of CER channel 5 (close to q = 3/2 from EFIT). (c) Flow shear across q = 3/2 as measured by CER, with and without smoothing over one energy confinement time. (d) m/n = 3/2 Mirnov amplitude with time. Colored time markers are for MRE evaluation before (green), during (red) and after (blue) increased amplitude period. (e) $-\Delta' r$ evaluated from the MRE at times noted in (d) versus the normalized flow shear at q = 3/2. The linear correlation is 0.74, σ is 0.081 and the best fit is $-\Delta' r = 1.1 \pm 0.1 + (3.6 \pm 3.0) \times NFS$. The dashed and solid horizontal lines are the average of the values before (and after) and during inversion, respectively.

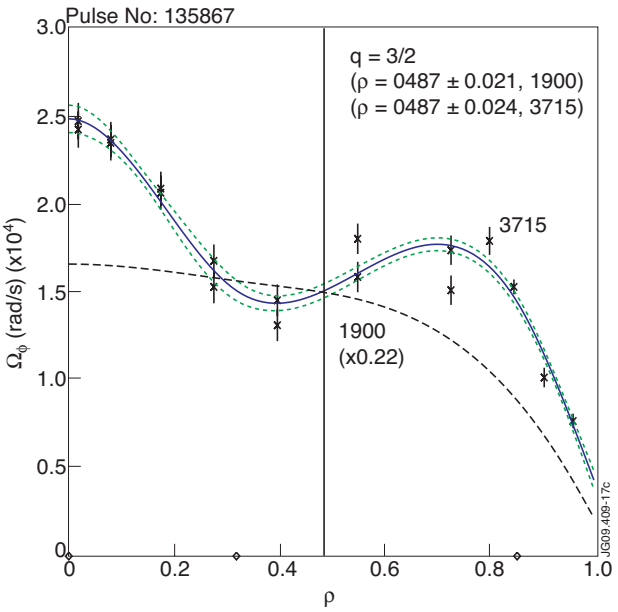

Figure 15: Solid line is fitted CER measure in DIII-D discharge 135867 of $\Omega_\phi(\rho)$ with ρ the normalized minor radius at t = 3715ms at large n = 2 Mirnov amplitude during inversion. Dashed lines are $\pm\sigma$. Dotted line is fit at t = 1900ms before torque sweep down, multiplied by 0.22 to scale for overlay.

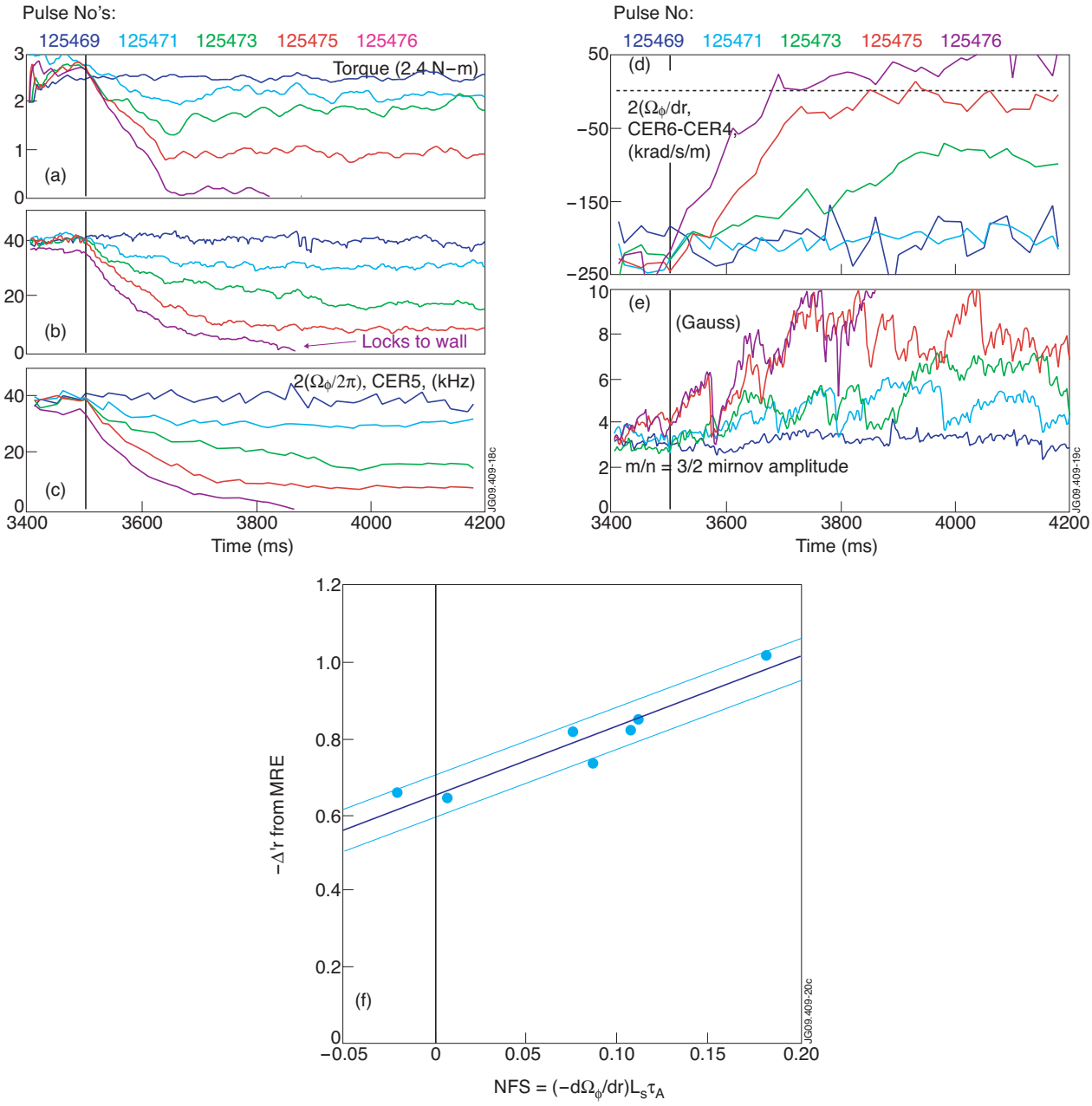

Figure 16: (a) Applied torque, (b) m/n = 3/2 Mirnov frequency, (c) twice the plasma rotation from CER channel 5 (closest to q = 3/2 from EFIT); DIII-D discharge 125476 is followed until the mode frequency goes to zero during wall locking, (d) flow shear from CER channels 6 and 4, (e) m/n = 3/2 Mirnov amplitude, (f) $-\Delta' r$ from MRE versus normalized flow shear; linear correlation is 0.93 and sigma is ± 0.052. Note that (e) includes two other redundant discharges not shown in (a)–(e).